ORIGINAL ARTICLE



Temperature and mass scaling affect cutaneous and pulmonary respiratory performance in a diving frog

Ryan B. MCWHINNIE, Jason P. SCKRABULIS and Thomas R. RAFFEL

Department of Biological Sciences, Oakland University, Rochester, Michigan, USA

Abstract

Global climate change is altering patterns of temperature variation, with unpredictable consequences for species and ecosystems. The Metabolic Theory of Ecology (MTE) provides a powerful framework for predicting climate change impacts on ectotherm metabolic performance. MTE postulates that physiological and ecological processes are limited by organism metabolic rates, which scale predictably with body mass and temperature. The purpose of this study was to determine if different metabolic proxies generate different empirical estimates of key MTE model parameters for the aquatic frog *Xenopus laevis* when allowed to exhibit normal diving behavior. We used a novel methodological approach in combining a flow-through respirometry setup with the open-source Arduino platform to measure mass and temperature effects on 4 different proxies for whole-body metabolism (total O2 consumption, cutaneous O₂ consumption, pulmonary O₂ consumption, and ventilation frequency), following thermal acclimation to one of 3 temperatures (8°C, 17°C, or 26°C). Different metabolic proxies generated different mass-scaling exponents (b) and activation energy (E_A) estimates, highlighting the importance of metabolic proxy selection when parameterizing MTE-derived models. Animals acclimated to 17°C had higher O2 consumption across all temperatures, but thermal acclimation did not influence estimates of key MTE parameters E_A and b. Cutaneous respiration generated lower MTE parameters than pulmonary respiration, consistent with temperature and mass constraints on dissolved oxygen availability, SA:V ratios, and diffusion distances across skin. Our results show that the choice of metabolic proxy can have a big impact on empirical estimates for key MTE model parameters.

Key words: African clawed frog, amphibian, pneumotachography, thermal biology

INTRODUCTION

Climate change is projected to increase mean temperatures and temperature variability, with potentially complex effects on species and the ecosystems they inhabit (Donelson *et al.* 2018; Morash *et al.* 2018; Burggren

Correspondence: Ryan B. McWhinnie, Oakland University, Department of Biological Sciences, 375 Dodge Hall, 118 Library Drive, Rochester, MI 48309, USA.

Email: rbmcwhin@gmail.com

2018). These changes are especially important for ectothermic animals including amphibians, which allow their core body temperatures to vary with environmental temperature. Understanding thermal responses is increasingly important for amphibians due to the global spread of temperature-dependent diseases (Berger *et al.* 1998; Stuart *et al.* 2004; Skerrat *et al.* 2007). Measuring how changes in temperature affect an organisms' physiological performance is crucial to identifying at-risk species and mitigating effects of anthropogenic climate change.

One of the most important tools for describing ectotherm thermal responses is the thermal performance

1

curve (TPC), which describes some metric of an organism's performance across a range of temperatures (Denny & Dowd 2012). TPCs are typically asymmetric and increase exponentially with temperature up to an organism's peak performance temperature (T_{pk}) , above which performance rapidly declines (Denny & Dowd 2012). Due to this inherent non-linearity of TPCs, it is important to quantify performance across a range of temperatures and to describe the TPC using an appropriate mathematical model. Although a wide variety of models have been used to describe thermal performance curves, arguably the most mechanistic and potentially generalizable are equations derived from the metabolic theory of ecology (MTE). Brown (2004) presents central equations, assumptions, and the theoretical framework in a greater depth.

One advantage of MTE-derived models is the potential generalizability of key model parameters such as the activation energy E_A , which is predicted to have similar values across taxa and physiological processes (Brown et al. 2004; Dell et al. 2011). Most MTE-derived models are parameterized using some proxy for metabolic performance (e.g. sprint speed, ventilation frequency, or activity level), which is assumed to be proportional to the massspecific metabolic rate B (Gillooly et al. 2001; Brown et al. 2004; Savage et al. 2007). However, this common assumption of a constant E_A across metabolic proxies remains to be tested for most ectotherm species. A second advantage of MTE-derived models is the ability to simultaneously describe temperature and mass-scaling effects on metabolism. Our goal in this study was not to test fundamental assumptions of MTE. Instead, we used MTE-derived models to simultaneously describe temperature and mass effects on respiratory performance in the model amphibian species *Xenopus laevis* (Daudin, 1802), and we tested the common empirical assumption of invariant $E_{\rm A}$ across multiple metabolic proxies. The first objective of this study was to estimate the E_A for wholebody metabolism of X. laevis and determine if different metabolic proxies generate similar E_A estimates.

An important aspect of TPCs is their ability to shift following extended exposure to a given temperature, due to developmental or reversible plasticity (i.e. thermal acclimation responses). Classic MTE studies tended to ignore acclimation effects on thermal performance curves (e.g. Gillooly et al. 2001), but more recent studies have suggested thermal acclimation can be incorporated into MTE by making key parameters into functions of recently experienced temperatures (Rohr et al. 2013). Depending on the type of response, acclimation temperature can have positive, negative, or non-linear effects

on the thermal performance curve (Altman et al. 2016; Padilla et al. 2019). The "beneficial acclimation" hypothesis predicts that acclimation of an organism to a given temperature will result in increased performance at that temperature, relative to unacclimated organisms (i.e. adaptive plasticity; Leroi et al. 1994). This type of pattern is typical for acclimation effects on ectotherm thermal limits (e.g. increased critical thermal maximum following warm-temperature acclimation; Bilyk & DeVries 2011). Results consistent with beneficial acclimation were observed for locomotor performance in X. laevis, where cold-acclimated frogs had higher maximum sprint speeds at cold temperatures relative to their warm-acclimated counterparts (Wilson et al. 2000; Seebacher et al. 2014). However, not all organisms or performance metrics exhibit beneficial acclimation responses when measured at temperatures below their $T_{\rm pk}$, instead exhibiting "cooler is better," "warmer is better," or "optimal temperature" responses (Wilson & Franklin 2002). The second objective of this study was to test for thermal acclimation effects on X. laevis metabolic performance and to determine if acclimation influence MTE parameter estimates. Based on the prior study on X. laevis swimming speed, we hypothesized a "beneficial acclimation" effect on X. laevis respiratory performance, which should be strongest immediately after a temperature shift and dissipate through time as each animal becomes acclimated to its new "performance" temperature.

Previous authors have demonstrated that withinspecies metabolic mass scaling relationships exhibit a wide range of exponents (here defined as parameter "b" in models), possibly due to differential reliance on specific physiological systems (reviewed by Glazier 2005, 2014a,b). For example, X. laevis is a diving frog that relies heavily on cutaneous respiration (gas exchange through the skin; Hutchison et al. 1968), which is temperature dependent and may be limited by the organism's surface area to volume ratio (SA:V; predicted scaling exponent of 2/3) or increased skin thickness in larger frogs (Rubner 1883; Greven et al. 1995; VanBuren et al. 2018). A prior study observed a mass-scaling exponent of 1.08 for X. laevis whole-body respiration, but frogs were taken out of their normal aquatic environment for measurements of oxygen consumption, possibly forcing them to rely more heavily than normal on pulmonary respiration (Hillman & Withers 1979). Furthermore, within-species mass scaling exponents have been found to change in response to temperature and thermal acclimation (Killen et al. 2010; Ohlberger et al. 2012). A third objective of this study was to estimate mass scaling exponents for X. laevis pulmonary, cutaneous, and whole-body respiration while allowing animals to exhibit their normal diving behavior, and to determine if temperature or thermal acclimation influences mass scaling relationships in this species. We hypothesized a scaling exponent for total O₂ consumption close to 0.75 (Savage *et al.* 2008), and a higher exponent for pulmonary than for cutaneous respiration due to constraints imposed by SA:V and skin thickness in larger frogs.

The focal species of this study was the African clawed frog Xenopus laevis, an amphibian species commonly used as a model organism in biomedical research. X. laevis is a diving frog that poses a unique set of challenges when studying respiration, due to its heavy reliance on cutaneous respiration and ability to go extended periods without surfacing to breathe air (pulmonary respiration; Boutilier 1984). A common methodological approach has been closed system respirometry (Hutchison & Miller 1979; Feder 1983; Hastings & Burggren 1995). However, other authors used pneumotachography, a specialized type of air flow-through system, to track ventilation frequency and measure breath volumes for diving animals including X. laevis (Boutilier 1984; Hedrick et al. 2011; Withers et al. 2014). Previous studies also measured whole-body metabolic rates by placing each frog in a humid air chamber (i.e. terrestrial environment) to generate a single value for whole-body oxygen consumption (Seymour 1973; Hillman & Withers 1979) or carbon dioxide production (Tsugawa 1982), or took separate measurements of changing oxygen concentrations in air and water to estimate relative contributions of pulmonary versus cutaneous respiration (Emilio & Shelton 1974, 1980; Hillman & Withers 1981; Feder & Wassersug 1984). Costs and limitations of these various respirometry systems for experiments with diving frogs are discussed in more detail in Supporting Information. A fourth objective of this study was to develop an inexpensive flow-through system for simultaneous measurement of total O₂ consumption, pulmonary O₂ consumption, cutaneous O₂ consumption, ventilation frequency, and breath volumes while allowing frogs to exhibit their normal diving behavior.

This study aimed to answer 3 key questions: (1) How does *X. laevis* whole-body metabolism scale with body mass, and does this mass-scaling exponent depend on the choice of metabolic proxy, temperature, or thermal acclimation status? (2) What is the activation energy estimate for *X. laevis* whole-body metabolism, and does this estimate depend on choice of metabolic proxy or thermal acclimation? (3) How does thermal acclimation affect the metabolic thermal performance curve of *X. laevis*, and do these effects differ for different metabolic prox-

ies? Answering these key questions will provide insights into the temperature dependence of *X. laevis* whole-body metabolism in a natural environment and help inform future studies of metabolic performance.

MATERIALS AND METHODS

Animal source and maintenance

All experiments were conducted in accordance with the Oakland University Institutional Animal Care and Use Committee (IACUC #18011).

Wild-type Xenopus laevis tadpoles (Nieuwkoop-Faber stages 56–63) were obtained in September of 2017 from a commercial research supplier (Nasco, Fort Atkinson, WI, USA) and raised to subadults (about 10 months old). The research supplier was unable to discern the strain of the species. All water quality parameters were maintained in accordance with optimal husbandry conditions presented by Green (2010). Groups of 15-30 tadpoles were housed in an opaque 2.4-gallon tank with gray-tinted translucent lids, to minimize potential distress from disturbance. Enrichment in the form of PVC pipes were used as refuge for social housing. Tanks were filled with 20°C Kordon Amquel®-treated water to slow the rate of water fouling. Animals were maintained on a 12:12 h light:dark cycle. Tadpoles were fed a crushed mix of "frog brittle" from the Xenopus supplier and changed daily. Subadults were housed in groups of 3 to 4 and fed3 times weekly with post-metamorphic brittle from the Xenopus supplier. All animals were checked daily for overall health and water quality.

Rationale for developing a custom flow-through system for diving-frog respirometry

We designed a new respirometry system to allow simultaneous measurement of cutaneous and pulmonary respiration in a diving frog, while allowing frogs to exhibit normal diving behavior. We based our design on a combination of respirometry strategies used by prior studies (Hillman & Withers 1979; Boutilier 1984; Fonseca *et al.* 2012; Tattersall *et al.* 2013). We considered it important to allow animals to exhibit normal diving behavior during respirometry measurements, to ensure that the relative contributions of cutaneous and pulmonary respiration (and their subsequent effects on overall MTE parameters) would be reflective of *X. laevis* in a more natural environment. We therefore chose not to force animals to

remain either fully submerged with no access to air or in a humid terrestrial chamber with no ability to submerge. Some prior studies used closed-system respirometry, in which O₂ concentrations are measured through time with no external source of oxygen, to track rates of cutaneous and pulmonary respiration in X. laevis (e.g. Hutchison & Miller 1979; Hillman & Withers 1979, 1981; Tattersall et al. 2013). However, we worried that depletion of atmospheric oxygen through time might influence X. laevis breathing behavior in our experiments, and we were concerned about possible toxicity of the mineral oil used by some prior studies to minimize oxygen diffusion between the air and water (e.g. Hillman & Withers 1981). We were also interested in tracking ventilation frequency and breath volumes as possible alternative metabolic proxies, which would not have been possible with closed system respirometry. We therefore sought a way to conduct flow-through respirometry for at least the pulmonary component of our respirometry system.

Some prior studies used pneumotachography to track breath rates and volumes in diving animals including X. laevis (Glass et al. 1983; Boutilier 1984; Fonseca et al. 2012). In these studies, animals were held within an upside-down funnel that restricted pulmonary respiration to a small "diving bell" (Glass et al. 1983; Boutilier 1984; Fonseca et al. 2012). Air was then pumped through the diving bell at a constant flow rate, which was measured using a pneumotachograph sensitive enough to pick up changes in flow rate caused by the animal's lung inspiration or expiration (e.g. Boutilier 1984). This setup has several advantages, in that it: (1) allows animals to exhibit their normal diving behavior, (2) ensures continuous access to freshly oxygenated air, (3) allows flow-through measurements of pulmonary O2 consumption (e.g. Fonseca et al. 2012), and (4) provides opportunities to restrict oxygen diffusion between water and air by limiting the surface area of water where animals breathe. However, these studies utilized analog flow spirometers that have become difficult to obtain and would likely not have been sensitive enough to measure breath volumes of some of the smaller frogs in the current study. Furthermore, commercially available flow-through respirometry systems that measure O₂ consumption were cost-prohibitive for our experimental design, which required measuring 12 animals simultaneously in replicate controlledtemperature chambers. We therefore sought to combine classic pneumotachography methods with a digital device capable of simultaneously measuring both the air flow rate and the oxygen concentration in the flow-through air over time.

Respirometry setup and quantifying metabolic proxies

We designed a respirometry system to simultaneously measure cutaneous and pulmonary respiration in a diving frog, inside a controlled-temperature incubator (Fig. 1; Fig. S1, Supporting Information), based on a combination of respirometry strategies used by prior studies (Hillman & Withers 1979; Boutilier 1984; Fonseca et al. 2012; Tattersall et al. 2013). Each animal was placed into a 1 L deli cup within a commercial reptile incubator (Exo Terra, www.exo-terra.com) set to the target performance temperature. We inserted an upside-down perforated funnel (top half of a plastic pop bottle) into each deli cup to restrict each animal's air access to a small (7 mL) pocket at the top of the funnel. Funnels were size matched to the body length of each frog to ensure they could reach the surface without needing to swim, thereby reducing background "noise" generated by frog swimming movements. However, it is important to recognize that water depth can influence X. laevis surfacing frequency (Shannon & Kramer 1988), with unknown effects on mass or temperature scaling of respiratory variables. Thus, it is possible that deeper water, which requires frogs to swim or float to reach the surface, might generate different results from the current study.

We pumped a constant flow of air through this air pocket during each respirometry measurement, at a rate of approximately 200 mL•min⁻¹, ensuring the air in the pocket was fully refreshed every 2-3 s. We connected the outgoing tube to our custom-built respirometry device to quantify of changes in air flow and oxygen percentages through time (Fig. 1). The device was sensitive enough to detect changes in air flow caused by frog inhalation and exhalation, each of which respectively decreased or increased the flow rate across the sensor, allowing us to count breaths through time and calculate individual breath volumes (Fig. S2, Supporting Information). Diving frogs like X. laevis typically have extended "gap" periods with no breaths punctuated by distinct periods of breathing activity (Boutilier 1984). Using Boutilier's (1984) terminology, we refer to these discrete periods of breathing activity as "breath bouts" and define one "breath" is a single cycle of inhalation and exhalation. We used these data to quantify pulmonary oxygen consumption for individual breaths and over the full measurement period. We also quantified cutaneous oxygen consumption by measuring changes in aqueous dissolved oxygen from the beginning to end of each measurement period. Additional details describing the respirometry setup and

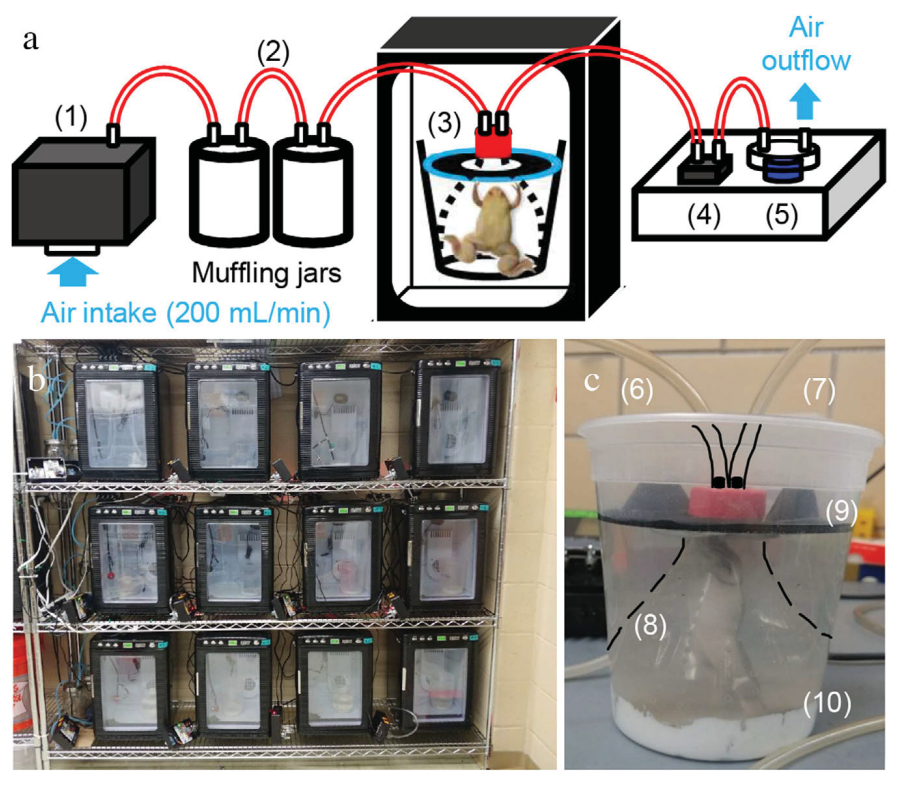


Figure 1 Complete respirometry setup. (a) Diagram of full respirometry setup including: (1) air intake pump, (2) a pair of quart-sized muffling jars used to minimize variation in flow rate going to the frog, (3) the frog within its pneumotachography setup (shown in panel "c"), (4) air flow-rate sensor, and (5) oxygen sensor covered by a modified plastic coin holder that channels air over the sensor. (b) Array of 12 incubators for performance temperature measurements of individual frogs. A black project box containing flow and O₂ sensors is visible to the left of each incubator, and muffling jars are visible to the left of each shelf. (c) Close-up photo of the pneumotachography setup for an individual frog including: (6) intake tubing for air going to frog, (7) outflow tubing from frog, (8) frog positioned vertically inside funnel (highlighted with dashed lines), (9) floating foam barrier to minimize oxygen diffusion between the water and air, and (10) sculpting clay to stabilize the funnel.

calculations for quantifying metabolic proxies can be found in Supporting Information.

Primary controlled-temperature experiment

Our primary experiment was designed to investigate effects of temperature and thermal acclimation on various metabolic proxies for *X. laevis*. A total of 24 subadult *X. laevis* were used for this study, though one frog died during the first acclimation period (i.e. maximum 23 frogs per experiment). We ran this experiment twice using the same set of frogs, re-randomizing each frog to a new temperature treatment combination prior to the second experiment. The mass and total body length (snout to tip of extended feet) of each frog was taken at the beginning and end of each 17-day acclimation period. Sizes varied from 13.13–59.95 g ($\underline{x} = 31.69$) for body mass and from 10.3–15.1 cm ($\underline{x} = 13.10$) for total

body length at the start of performance measurements. We did not determine animal sex because frogs were too young to exhibit external characteristics of sexual maturity. Each of the 2 experiments was further divided into 2 temporal blocks for measurement purposes, since only a maximum of 12 frogs could be measured simultaneously. Experiment 1 (blocks 1 & 2) was conducted in late June of 2018 and experiment 2 (blocks 3 & 4) was conducted in late July of 2018. All measurements were conducted during typical workday hours, ranging from morning to midafternoon. Animals were randomly assigned to blocks and temperature treatments. Animal identifications were maintained throughout the entirety of this study, allowing us to control for random effects of individual frogs. Each experiment began with a 17-day acclimation period in which animals were acclimated to 8°C, 17°C, or 26°C. Within each temporal block, we measured frog respiration at 5 time points relative to the

end of the acclimation period: -1, 0, 1, 4, and 8 days. At the end of the acclimation period (day 0), each animal was shifted to one of 8 randomly assigned performance temperatures for respirometry measurements (8°C, 11°C, 14°C, 17°C, 20°C, 23°C, 26°C, and 29°C). During the performance period (0–8 day time points), performance temperatures were re-randomized for each respirometry measurement, with constraints to not repeat the same performance temperature for a given frog within each experiment. This experimental design minimized the possibility of frogs becoming acclimated to their new performance temperatures. Further experimental design details are provided in Supporting Information.

Post-experiment measurements

The primary controlled-temperature experiment included a sufficiently broad range of animal masses to reveal interesting differences in mass scaling coefficients among metabolic proxies (13.13–59.95; $\underline{x} = 30.65$). However, this mass range is less than the order of magnitude, which might result in inaccurate intraspecific estimates of parameter "b" due to the potential for curvilinear mass-scaling relationships (Savage *et al.* 2008). To generate more accurate estimates of b for various metabolic proxies, we collected additional measurements from 8 recently metamorphosed X. laevis frogs in a smaller size range (1.87–3.18 g, \underline{x} = 2.66). To obtain comparable measurements, we randomly assigned each frog to one of the performance temperatures from the original controlled-temperature experiment.

Statistical analyses

All statistical analyses were based on linear mixedeffects regression (lmer function from the lme4 package) and conducted using R statistical software v. 3.5.1 (R Core Team 2018), allowing us to incorporate random effects of Acclimation incubator, Performance incubator, and Frog identity into statistical models. The random effect of Frog identity was nested within the effect of Acclimation incubator. We natural log-transformed all response variables (i.e. our 4 metabolic proxies) and used the inverse of performance-temperatures (in degrees Kelvin) as a primary explanatory variable, to allow estimation of E_A from linear-model outputs both in the overall controlled-temperature experiment and for each individual time point. We also included natural log-transformed body mass as a covariate in each model, to account for mass-scaling effects and to allow estimation of the massscaling exponent (b) for each metabolic proxy. For analysis of the primary controlled-temperature experiment, we also tested for curvilinear and interactive effects of acclimation temperature and time since the temperature shift. Further details about model structure are provided in Supporting Information Supplementary Methods.

To determine if MTE parameter estimates depended on the size range of animals included in the analysis, we re-ran linear mixed effects models with and without inclusion of post-experiment measurements collected from frogs in a smaller size range. These models were simplified to remove fixed effects of acclimation temperature or time because all of the smaller frogs used for post-experiment measurements had been acclimated to the same temperature (19°C). However, we retained the random-effects structure from the original mixed-effects models. The new frogs were all assigned to the same "acclimation incubator" for the purpose of accounting for this random effect, since they were maintained on the same shelf in our animal room prior to conducting measurements.

RESULTS

Acclimation effects on thermal performance

To test for potential linear or curvilinear effects of acclimation temperature on each metabolic proxy, we focused on data from time points following the acclimation period. We began by testing for time by temperature interactions using the full time series (days 0–8; Table 1; Fig. S3, Supporting Information). We detected a statistically significant positive 3-way interaction for effects of inverse performance temperature × time × quadratic acclimation temperature on total O2 consumption. We also detected a significant quadratic acclimation temperature x time interaction for total O₂ consumption, revealing negative curvilinear effects of acclimation at a large time scale. Cutaneous respiration also generated a significant positive quadratic acclimation \times time interaction (Table 1). A main effect of time on ventilation frequency was statistically significant, revealing that ventilation frequency increased through time post-acclimation (Table 1). We next conducted a series of focused models examining each individual time point (days 0, 1, 4, and 8), to determine if acclimation effects were stronger at time points immediately following the temperature shift (Table S1 and Fig. S4, Supporting Information). Immediately following the temperature shift, there was a trend towards a quadratic effect of acclimation on total oxygen consumption (P =0.088; Table S1, Supporting Information; Fig. 2a). These patterns were supported by highly significant interactions

Table 1 Linear mixed-effects models testing for effects of acclimation through time (days 0–8), in the primary controlled-temperature experiment

Response	Predictor	$Coef \pm SE$	F	df	P
Total O ₂	PerfTemp ⁻¹	0.458 ± 0.029	260.2	1, 157.0	< 0.001
	АссТетр	0.003 ± 0.006	0.1	1, 7.6	0.783
	AccTemp ²	$-3.55 \times 10^{-4} \pm 0.001$	0.1	1, 7.0	0.751
	ln Mass	0.430 ± 0.124	10.6	1, 37.6	0.002
	Time	0.006 ± 0.007	0.8	1, 137.0	0.381
	$PerfTemp^{-1} \times AccTemp$	19.1 ± 44.2	0.3	1, 161.8	0.610
	$PerfTemp^{-1} \times AccTemp^2$	6.25 ± 8.61	0.6	1, 158.7	0.458
	$PerfTemp^{-1} \times Time$	0.732 ± 115.0	0.0	1, 151.5	0.953
	AccTemp × Time	$8.36 \times 10^{-4} \pm 0.001$	0.7	1, 145.1	0.405
	$AccTemp^2 \times Time$	$6.67 \times 10^{-4} \pm 2.01 \times 10^{-4}$	10.8	1, 147.5	0.001
	$PerfTemp^{-1} \times AccTemp \times Time$	-0.101 ± 15.32	0.0	1, 171.2	0.976
	$PerfTemp^{-1} \times AccTemp^2 \times Time$	7.37 ± 3.50	3.9	1, 107.8	0.049
Cutaneous O ₂	PerfTemp ^{−1}	0.278 ± 0.020	196.1	1, 171.2 1, 107.8 1, 181.0 1, 8.6 1, 7.5	< 0.001
	АссТетр	0.006 ± 0.004	2.0	1, 8.6	0.193
	AccTemp ²	$-4.48 \times 10^{-4} \pm 8.16 \times 10^{-4}$	0.3	1, 7.5	0.610
	ln Mass	0.270 ± 0.085	8.9	1, 37.2	0.005
	Time	0.012 ± 0.005	4.9	1, 155.7	0.029
	AccTemp × Time	$1.04 \times 10^{-4} \pm 7.20 \times 10^{-4}$	0.1	1, 98.6	0.739
	$AccTemp^2 \times Time$	$4.27 \times 10^{-4} \pm 1.40 \times 10^{-4}$	9.0	1, 160.8	0.003
Pulmonary O ₂	PerfTemp ^{−1}	0.794 ± 0.066	119.2	1, 168.6	< 0.001
	АссТетр	-0.004 ± 0.012	0.1	1, 9.5	0.760
	ln Mass	0.768 ± 0.238	9.3	1, 39.3	0.004
	Time	0.004 ± 0.017	0.1	1, 138.2	0.803
Ventilation frequency	PerfTemp ^{−1}	0.365 ± 0.062	26.0	1, 215.8	< 0.001
	АссТетр	-0.018 ± 0.012	2.0	1, 9.7	0.188
	ln Mass	0.098 ± 0.247	0.1	1, 39.8	0.709
	Time	0.042 ± 0.016	6.9	1, 140.4	0.010

Statistical tests are based on linear mixed effects regression, using F-tests with type II sums of squares and Kenward-Rogers df. All models included random effects of performance incubator, acclimation incubator, and frog identity. Final models were selected using backwards selection, with non-significant interaction terms removed (P > 0.05). Time was measured from the day each frog was moved to its final performance temperature (0, 1, 4, and 8 days). Predictor coefficients were taken from models with only marginal terms removed, to ensure they could be used to interpret main effect directionalities. PerfTemp $^{-1}$ A estimates in other tables. Coefficients were multiplied by -k for comparison with E_A .

between time and the quadratic effect of acclimation temperature for total oxygen consumption and cutaneous respiration, consistent with an "optimum temperature"-type acclimation pattern.

No other metabolic proxies revealed significant acclimation effects on day 0. A statistically significant positive effect of acclimation was detected on day 1 for cutaneous respiration (Table S1, Supporting Information). Cold-

acclimated animals had the lowest levels of cutaneous respiration across performance temperatures, which likely drive this pattern (Fig. 2b).

We detected a strong negative trend of acclimation effects on ventilation frequency at 1 day into the performance period (Table S1, Supporting Information), with warm-acclimated animals having lower ventilation frequency levels across all performance temperatures. No

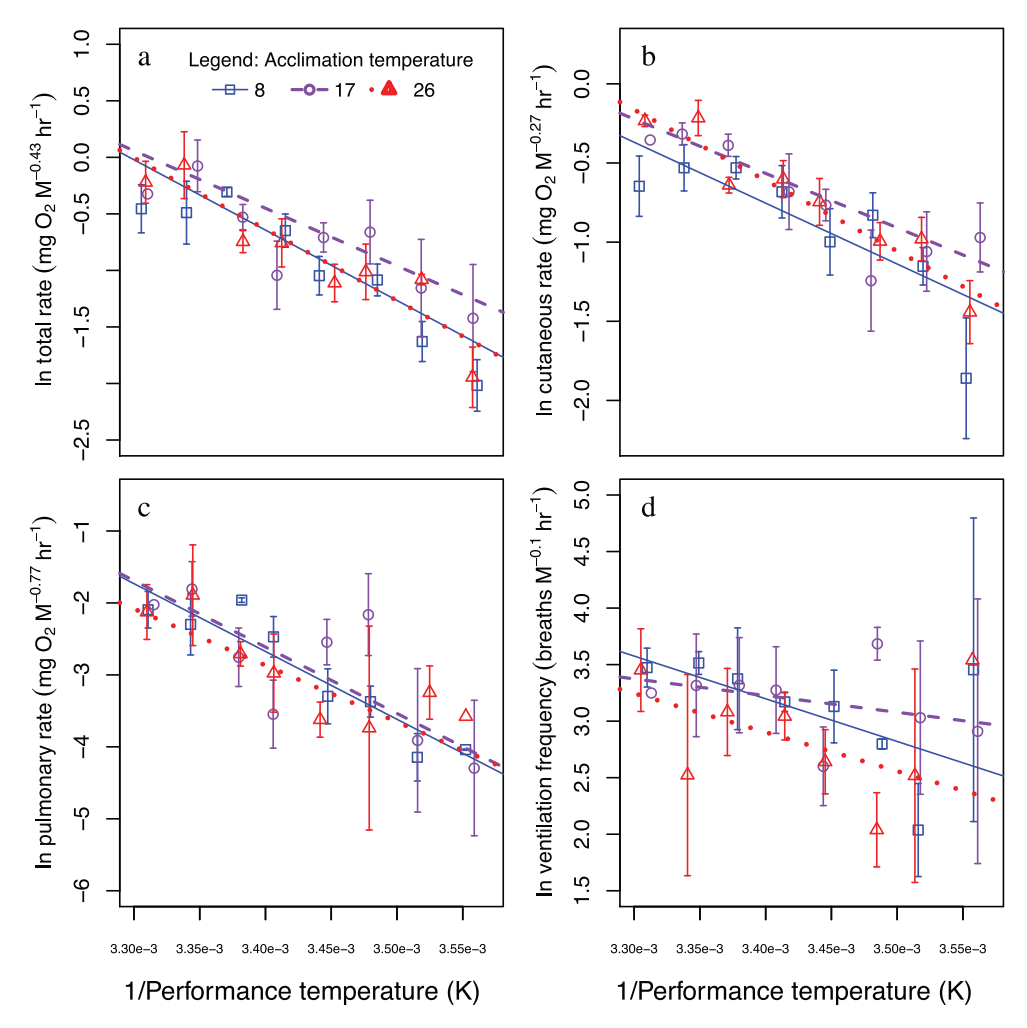


Figure 2 Thermal performance curves for all metabolic proxies on day zero of the primary controlled-temperature experiment (i.e. immediately following the shift from acclimation temperatures). (a) Total respiration (N = 75). (b) Cutaneous respiration (N = 81). (c) Pulmonary respiration (N = 72). (d) Ventilation frequency (N = 72). All response variables were natural log transformed and scaled according to the observed mass scaling effects. Note that the lines for cold- and warm-acclimated animals overlap in panel (a). Error bars represent the standard error of each treatment group containing N > 1 replicates.

significant effects of acclimation were detected for any metabolic proxy at 4 or 8 days following the temperature shift (Table S1, Supporting Information).

MTE parameter estimates: Mass scaling exponents (b) and activation energies (E_A)

To maximize the number of measurements used to generate estimates of key MTE parameter estimates (overall b and E_A values), we used data collected at all time points post-acclimation, including measurements from the primary controlled-temperature experiment and additional measurements of 8 smaller frogs. Parameter estimates are

provided as mean followed by 95% confidence intervals. All 4 metabolic proxies increased with body mass, resulting in positive mass scaling exponents (Fig. 3; Table S2, Supporting Information). Pulmonary respiration had a higher mass-scaling exponent (b = 1.565; 95% CI 1.311-1.819) than cutaneous respiration (b = 0.472; 0.372-0.571), resulting in an intermediate value for total O₂ consumption (b = 0.690; 0.576-0.803). Ventilation frequency generated the lowest mass-scaling exponent (b = 0.225; 0.004-0.445). We detected no statistically significant interactions of mass with either acclimation or performance temperature. Final estimates of mass-scaling exponents for pulmonary, cutaneous, and total respiration all increased with addition of the 8 smaller frogs,

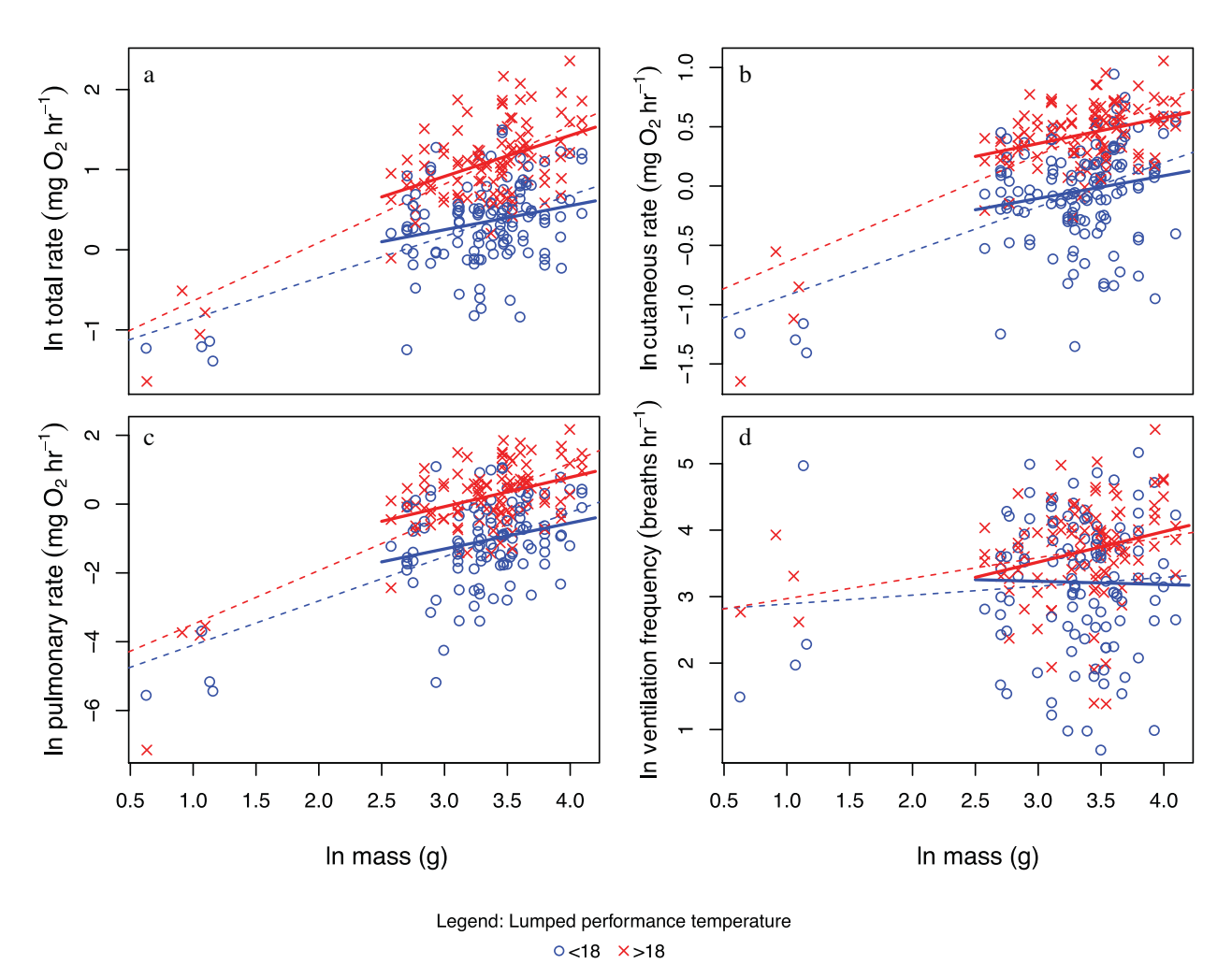


Figure 3 Plots of all 4 metabolic proxies as a function of frog mass on a log-log scale for all measurements, including 8 smaller frogs that were not part of the original controlled-temperature experiment. (a) Total O_2 consumption (N = 236), (b) cutaneous O_2 consumption (N = 257), (c) pulmonary O_2 consumption (N = 236), and (d) ventilation frequency (N = 237). Data are grouped according to performance temperature ($<18^{\circ}$ C: blue circles; $>18^{\circ}$ C: red crosses). Note that best-fit lines were generated using simple linear regression to illustrate trends and do not account for random effects, unlike the statistical models we used to estimate MTE parameters. Solid lines were generated based on the original dataset from the primary controlled-temperature experiment. Dashed lines were generated using the full dataset.

relative to estimates based only on data from the primary controlled-temperature experiment (Table S2, Supporting Information).

Total O_2 consumption (pulmonary plus cutaneous) and ventilation frequency yielded intermediate E_A estimates of 0.444 eV (0.389–0.499) and 0.373 eV (0.250–0.496), respectively (Table S2, Supporting Information). Pulmonary respiration yielded the highest overall E_A estimate (0.770 eV; 0.640–900) relative to other metabolic proxies, whereas cutaneous respiration alone yielded the lowest estimate (0.270 eV; 0.213–

0.309). Ventilation frequency revealed a trend towards a curvilinear performance temperature \times quadratic effect of acclimation temperature interaction ($F_{1,155.8} = 3.0$; P = 0.088; Table 1), driven by an apparently lower E_A for 17°C-acclimated frogs (0.102 eV; -0.144-0.348) relative to cool-acclimated (8°C: 0.488 eV; 0.306–0.669) or warm-acclimated frogs (26°C: 0.444 eV; 0.231–0.657). Unlike with the mass-scaling exponents, additional measurements from frogs in a smaller size range had little effect on the estimated E_A for any of the 4 metabolic proxies (Table S2, Supporting Information).

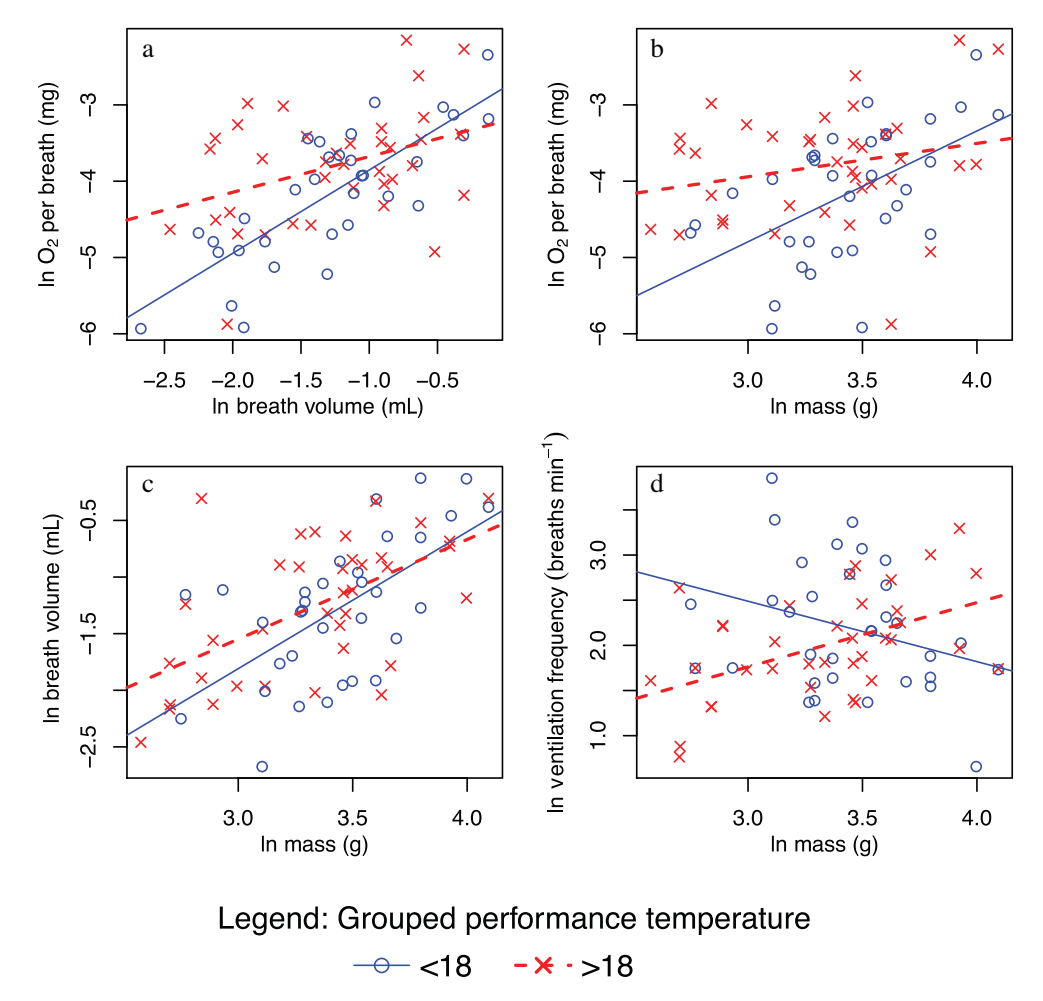


Figure 4 Mass- and volume-scaling relationships on a per-breath log-log scale, for breath bout data from the primary controlled-temperature experiment. Performance temperatures are grouped ("Cool" temperatures [8°C, 11°C, 14°C, and 17°C]; "Warm" temperatures [20°C, 23°C, 26°C, and 29°C]) for ease of data visualization. Panels show relationships between: (a) Breath volume and oxygen consumption (N = 65.7); (b) mass and oxygen consumption (N = 38.7). (c) Mass and breath volume (N = 38.6); (d) mass and ventilation frequency (breaths per minute; N = 38.6).

Mass- and volume-scaling relationships for individual breaths

To examine scaling relationships between breath volume, pulmonary O_2 consumption, and body mass in the original controlled-temperature experiment, we generated a separate dataset to focus on individual breath bouts for a given frog. We used this dataset to analyze scaling patterns for individual breath, providing an indirect way to assess how well breath volume might have worked as a fifth metabolic proxy. We first examined the scaling relationship between individual breath volume and O_2 uptake per breath to determine whether these variables were directly correlated with each other. However, this analysis

revealed a strong interaction between breath volume and performance temperature, indicating that the scaling relationship between these 2 parameters was temperature-dependent (Table S3, Supporting Information). Oxygen uptake per breath increased faster with breath volume at cooler temperatures than at warmer temperatures (Fig. 4a; Table S4, Supporting Information). Given the absence of a temperature effect on the scaling exponent for overall pulmonary respiration through time (Table 1), this result initially seemed to suggest that using breath volume through time as a metabolic proxy might have generated a temperature-dependent mass scaling relationship.

We followed up on this result by examining relationships between log-transformed body mass (M), O_2 uptake

per breath, individual breath volume, and ventilation frequency within the breath bout dataset. Temperature interacted with ln(M) to affect O_2 uptake per breath (Fig. 4b; Table S3, Supporting Information), paralleling the interactive effects of temperature and breath volume on O₂ uptake per breath (Fig. 4a; Table S3, Supporting Information). In both cases, the interaction was driven by smaller frogs (or smaller breaths) absorbing more O₂ per breath at warmer than at cooler temperatures. In contrast, temperature did not significantly interact with the ln(M) effect on individual breath volume (Table S3, Supporting Information), although we detected a trend toward a $ln(M) \times performance$ temperature interaction (P = 0.081). Furthermore, In breath volume was almost directly proportional to ln(M) with a scaling coefficient statistically indistinguishable from 1.0 (Table S3, Supporting Information). These results indicate that the temperature × breath volume interaction was driven by increased O2 uptake at warmer temperatures for smaller frogs, rather than a temperature effect on individual breath volumes.

We also examined potential effects of acclimation and performance temperature on relationships between individual breath volume, oxygen uptake per breath, body mass (M), and ventilation frequency in the breath bout dataset (Table S3, Supporting Information; Fig. 4). The only statistically significant effect of acclimation temperature in the individual-breath analyses was a positive main effect on ventilation frequency (P = 0.040)after accounting for the effect of mass and performance temperature. Performance temperature decreased the scaling exponents for effects of both individual breath volume (Fig. 4a) and body mass (Fig. 4b) on oxygen uptake per breath, as indicated by significantly negative interactive effects between ln(M) or $ln(V_{Breath})$ and performance temperature (Table S3, Supporting Information).

There was no significant interactive effect of $\ln(M)$ and performance temperature on individual breath volume (Fig. 4c; Table S3, Supporting Information). In contrast, performance temperature increased the scaling exponent for the effect of body mass on ventilation frequency (Fig. 4d), as indicated by a significantly positive interactive effect of $\ln(M)$ and performance temperature on ventilation frequency in the breath bout dataset (Table S3, Supporting Information). Note that this same interactive effect of $\ln(M)$ and performance temperature was not significant in a separate mass-scaling analysis of individual breaths with the full dataset (discussed above; Table 1), though there was a trend towards a similar interactive effect in the same direction.

Observations of breathing behavior

Frogs exhibited patterns of breathing behavior similar to those observed in previously published experiments. Individual ventilations typically started with an exhalation followed by an immediate inhalation, as described by Brett and Shelton (1979; Fig. S2c, Supporting Information). As described by Boutilier (1984), frogs tended to ventilate their lungs multiple times each time they surfaced for air, with some frogs remaining near the surface and breathing in regular bouts ("bout breathing" behavior; Fig. S5a, Supporting Information) and others surfacing for a rapid succession of many ventilations following long periods without breathing ("burst breathing" behavior; Fig. S5b, Supporting Information). In general, frog breath rates tended to be faster at warmer temperatures and for larger frogs, across a range of breath rates consistent with those observed by Boutilier (1984; Table S5, Supporting Information).

DISCUSSION

Mass scaling exponents

Metabolic mass-scaling relationships varied depending on the metabolic proxy examined (Table 1) and the mass range of the frogs examined (Table S2, Supporting Information). The most direct measurement for whole-body metabolism in this study was total oxygen consumption, for which the full dataset generated a mass scaling exponent (b) similar to the MTE-predicted M^{0.75} power law (Brown et al. 2004; b = 0.690; 95% CI 0.576–0.803). This estimate approximates the mean scaling coefficient observed in other empirical studies of intraspecific mass scaling (Hutcison et al. 1968). This scaling exponent for total respiration was intermediate between the estimates for cutaneous (b = 0.472; 0.372–0.571) and pulmonary (b = 1.565; 1.311-1.819) respiration. All 3 of these estimates were substantially increased when we added measurements from smaller frogs that were not part of the original controlled-temperature experiment (Table S1, Supporting Information), consistent with prior observations of convex curvature for intraspecific mass-scaling relationships and emphasizing the importance of including at least an order of magnitude range of masses when estimating intraspecific mass scaling parameters (Table S2, Supporting Information; Fig. 3; Savage *et al.* 2008).

We observed the largest mass-scaling exponent (b) for pulmonary oxygen consumption, which also exhibited the greatest increase in b with addition of the smaller frogs (Table S2, Supporting Information). This is apparently because larger frogs relied much more heavily on

pulmonary respiration than smaller frogs (Fig. S6, Supporting Information). This makes biological sense, because larger frogs have a lower surface-area to volume (SA:V) ratio than smaller frogs and should be less able to meet their oxygen demands via cutaneous respiration alone. As frogs get larger and rely more heavily on pulmonary respiration, you would expect the pulmonary scaling coefficient to begin converging on the overall *b* for total oxygen consumption. This is essentially what we saw when we focused on the larger frogs from the original experiment: a scaling coefficient for pulmonary respiration only slightly higher than 0.75 (Table S2, Supporting Information).

Cutaneous-only respiration generated a mass-scaling exponent that was lower than total or pulmonary respiration, and somewhat lower that the M^{2/3} exponent predicted by a classic surface-area to volume (SA:V) scaling relationship (Rubner 1883; White & Seymour 2003; Table 1). A combination of biological factors likely influenced this depression in the mass-scaling exponent relative to other metabolic proxies. Gillooly et al. (2016) showed that mass scaling exponents for respiration are generally limited by how the respiratory surface area (i.e. skin surface area) and diffusion distance (i.e. skin thickness) scale with mass, with b equaling the difference between these 2 exponents. To our knowledge, there is no published work that simultaneously measured body mass, skin surface area, and skin thickness (or any combination of these 2 variables) in X. laevis, so we were unable to directly compare the mass scaling exponent for cutaneous respiration to exponents for surface area or skin thickness. However, X. laevis has a body shape similar to other anurans rather than possessing specific adaptations to increase skin surface area, and Hutchison et al. (1968) found that the average mass-scaling exponent for surface area across several anuran species was M^{0.58}. This is lower than the theoretical surface area to volume b of 0.67 for a spherical object (Rubner 1883), and only slightly outside the 95% c.i. for the cutaneous-respiration scaling coefficient observed in this study. Furthermore, X. laevis skin thickness appears to increase with body size, based on prior studies showing that females have both larger body mass and thicker skin than males (Greven et al. 1995; VanBuren et al. 2018). Based on these findings, a combination of SA:V and skin-thickness scaling relationships can likely account for the lower-than-expected mass-scaling exponent for cutaneous respiration observed in this study.

As expected, ventilation frequency generated the lowest *b* for all 4 metabolic proxies (Table 1; Table S2, Supporting Information). Because ventilation frequency is a

mass-specific metabolic process, MTE predicts that the mass-scaling exponent should be 1.0 less than that for whole-body metabolic rate. In the present study, we predicted that the ventilation frequency mass-scaling exponent would be 1.0 less than the pulmonary mass-scaling exponent because these 2 metabolic proxies are inherently interrelated (i.e. 1.57 - 1.0 = 0.57). The estimate of the X. laevis ventilation frequency exponent was somewhat smaller than this predicted value, though with overlapping confidence intervals (0.311–0.819 vs 0.004–0.445; Table S2, Supporting Information). One potential reason for discrepancies between the pulmonary and ventilation frequency mass-scaling exponents is that there was a substantial amount of noise in the flow rate time-series data, usually caused by sudden animal movements within the respirometry setup. These fluctuations generally lacked the distinguishing characteristics of real breaths, but they also frequently obscured real breaths, making it difficult to obtain accurate breath counts from the full time series of many frogs. As a result, this was an important source of measurement error in the "breath bout" dataset derived from the full time series for each frog. This noise also prevented us from obtaining accurate measurements of total ventilation volume through time, which we originally planned to analyze as a fifth metabolic proxy. We therefore explored the potential use of ventilation volume as an alternative metabolic proxy by examining mass-scaling relationships for the volume of individual breaths using the breath bout dataset, as described below.

All 4 metabolic proxies here analyzed generated different estimates of *b* for *X. laevis*, emphasizing the importance of selecting an appropriate metabolic proxy when investigating mass-scaling relationships for wholebody metabolism. However, these differences were qualitatively consistent with MTE predicted mass scaling relationships, and they might have been possible to predict quantitatively given sufficient information about how *X. laevis* skin surface area and thickness change with body mass (Gillooly *et al.* 2016). Importantly, there were no significant effects of temperature or thermal acclimation on mass-scaling exponents derived from any of the 4 metabolic proxies.

Mass- and volume-scaling relationships for individual breaths

If temperature influences the mass-scaling relationship for O_2 uptake per breath (Fig. 4a,b), then why did we not see a similar temperature-dependence for the mass scaling of pulmonary respiration in our full analysis (Fig. 3c)? The answer seems to have been that temperature had the

opposite interactive effect on the mass-scaling relationship for ventilation frequency, at least within the breath bout dataset (Table S4, Supporting Information; Fig. 4d). Indeed, reexamination of the ventilation frequency analysis from the full dataset revealed a similar trend towards temperature-dependent mass scaling (Fig. 3d), though this effect was non-significant (Table 1). These effects of temperature on b for O_2 per breath and ventilation frequency appear to have canceled each other out, with smaller frogs absorbing more O_2 per breath at warmer temperatures but breathing less frequently (Fig. 4b,d), ultimately resulting in a temperature-independent b for pulmonary O_2 consumption through time (Fig. 3c).

Activation energy estimates

As expected, activation energy estimates for all metabolic proxies fell within the reported range of 0.1– 1.0 across taxa (Gillooly et al. 2001; Brown et al. 2004), with no statistical evidence for thermal acclimation effects on E_A . This finding corroborates current prominent MTE literature (Dell et al. 2011). Importantly, E_A estimates remained similar whether or not our analysis included the smaller frogs whose measurements were obtained after the primary controlled-temperature experiment (Table S2, Supporting Information). However, we found that estimates of the key metabolic parameter E_A varied considerably for X. laevis depending on which metabolic proxy we focused on. Most prior studies have generated E_A estimates based on only one metabolic proxy at a time (Nagano & Ode 2014). Obtaining different activation energies for the same species based different performance metrics might be interpreted to reflect fundamental differences in the temperature-dependence of different physiological processes, perhaps due to the involvement of different rate-limiting enzymes. However, results from the current study suggest that even direct measures of oxygen consumption can generate divergent estimates for the same organism's metabolic activation energy, particularly if one fails to account for all sources of oxygen (e.g. cutaneous versus pulmonary respiration). Based on this and prior studies for X. laevis and other amphibians (Whitford 1973; Hutchison & Miller 1979), reliance on pulmonary respiration increases at warmer temperatures, likely due in part to decreased dissolved oxygen availability in water at warmer temperatures (Fig. S7, Supporting Information; Keeling & Garcia 2002). This resulted in pulmonary oxygen uptake increasing with temperature more rapidly than cutaneous oxygen uptake, leading to a subsequently higher E_A estimate for pulmonary respiration.

Ventilation frequency also generated an intermediate $E_{\rm A}$ estimate, similar to total ${\rm O_2}$ consumption. This was contrary to our a priori prediction that ventilation frequency would generate an $E_{\rm A}$ estimate similar to that of pulmonary oxygen uptake because of close biological relationship between these 2 metabolic proxies. This discrepancy is at least partly explained by our finding that frogs absorbed more oxygen per breath at warmer temperatures than at cooler temperatures, as revealed by positive main effect of temperature in the breath bout analysis. This effect might somewhat decrease the need for faster ventilation frequencies at warmer temperatures, relative to the need for increased pulmonary oxygen resulting in a lower $E_{\rm A}$ estimate for this proxy.

Acclimation effects on thermal performance

We found evidence of an optimal temperature-type thermal acclimation effect on the X. laevis whole-body metabolic rate, based on an analysis of total O2 consumption (Table 1). This acclimation effect could be modeled in an MTE framework by allowing the normalization constant to be a function of acclimation temperature, as suggested by Gillooly et al. (2006). Overall, frogs acclimated to 17°C had higher O₂ consumption on day 0 than those acclimated to 8°C or 26°C (Fig. 2a), and this effect decreased through time following the temperature shift as indicated by a significant interaction between time and the quadratic effect of acclimation temperature (Fig. S4, Supporting Information; Table 1). However, the magnitude of this acclimation effect was weak and not statistically significant for individual time points, despite a strong trend towards a quadratic effect of acclimation temperature on day 0 (Table S1, Supporting Information). Analysis of other metabolic proxies revealed similar evidence of acclimation responses for cutaneous but not pulmonary O₂ consumption, suggesting that any effects of thermal acclimation on total O₂ consumption were driven by changes in cutaneous respiration.

This evidence for an optimal temperature-type acclimation response contrasts with results of prior studies, which measured acclimation effects on swimming speed and muscle power in *X. laevis* (Wilson *et al.* 2000; Seebacher *et al.* 2014). Both studies found evidence of higher performance by cold-acclimated animals when measured at cooler temperatures, consistent with either a beneficial acclimation or a cooler-is-better type response. Neither study included a third acclimation temperature, leaving open the possibility that either study might have detected decreased performance at even colder temperatures (i.e. an optimal temperature response). However,

"cold acclimation" occurred at 10°C in Wilson *et al.* (2000) and 15°C in Seebacher *et al.* (2014), and in both cases, cold-acclimated frogs outperformed warmacclimated (25°C) frogs at cooler performance temperatures. In contrast, frogs acclimated to 8°C and 25°C in the current study appear to have had similarly low metabolic performance compared to 17°C acclimated frogs. These different results suggest that thermal acclimation has different effects on specific physiological processes (e.g. muscle performance) than on whole-body metabolic performance.

CONCLUSIONS

The results of this study show that the choice of metabolic proxy can influence estimates of key MTE parameters, and that X. laevis metabolic performance is influenced by thermal acclimation. All observed E_A estimates fell within the reported range for most animal taxa (Gillooly et al. 2001; Brown et al. 2004) but varied depending on the metabolic proxy examined, with pulmonary respiration generating a higher E_A value than cutaneous respiration due to a shift from cutaneous to pulmonary respiration at warmer temperatures. We also found evidence of an optimal-temperature type acclimation effect on the X. laevis whole-body metabolic rate, with higher total and cutaneous O₂ consumption in frogs acclimated to an intermediate temperature. This study also emphasizes the importance of allowing animals to exhibit normal respiratory behavior when studying mass and temperature effects on metabolic rates.

The observed mass-scaling exponent for total O₂ consumption of X. laevis was statistically indistinguishable from the MTE-predicted value of 0.75 (Gillooly et al. 2006), and the observed mass-scaling exponent for cutaneous respiration was only slightly less than the mean SA:V scaling exponent observed in a prior studies of frog morphology (0.58; Hutchison et al. 1968). This finding suggests that X. laevis cutaneous respiration is limited by skin surface area and SA:V ratios, and that larger frogs compensate for reduced SA:V by relying more on pulmonary respiration. Most prior studies of allometric scaling in diving animals focused on amniote vertebrates, which rely exclusively on pulmonary respiration (Schreer & Kovacs 1997; Halsey et al. 2006), though a prior study of bullfrogs also showed that increased temperatures led to greater reliance on pulmonary O2 uptake and CO2 elimination (Gottlieb & Jackson 1976). It would be interesting to examine b in other air-breathing diving species with significant cutaneous respiration (e.g. other aquatic frogs and salamanders) to determine if this is a common adaptation to a diving lifestyle. All of our estimated mass scaling exponents increased after incorporating additional measurements of smaller frogs. This result highlights the importance of including a wide range of masses for estimating intraspecific mass-scaling coefficients (Glazier 2005, 2010), preferably more than 1 order of magnitude as recommended by Savage *et al.* (2008). Had we stuck with the original mass range (13–60 g; about fivefold), we would have substantially underestimated the mass scaling estimates for all of our metabolic proxies. Including the additional measurements of smaller frogs makes these findings more robust and generalizable, for potential comparison with other diving species that exhibit significant amounts of cutaneous oxygen consumption.

The Arduino-based respirometry device developed in this study provides a powerful new experimental tool that may facilitate future experimental work. In the current study, this device made it possible to conduct flow-through respirometry with up to 12 animals simultaneously, facilitating quantification of metabolic thermal performance curves and acclimation effects. Furthermore, we were able to quantify breath volumes and oxygen uptake for individual breaths, allowing examination of allometric relationships at an individual breath level. Importantly, all measurements were collected while allowing animals to exhibit their normal diving behavior, generating more ecologically relevant estimates for b and E_A than would otherwise have been possible. Future researchers may find new ways to apply these tools to answer questions that might otherwise have been experimentally intractable.

ACKNOWLEDGMENTS

We thank the editor for their feedback and ultimately pushing us to produce a more robust and impactful contribution. The authors would also like to thank A. Orille, H. Russell, S. Pelton, B. Walter, K. Julius, J. Williams, and L. Trumbore for assisting with animal maintenance and preliminary experiments; A. Orille, S. Pelton, B. Walter, and M. Ostrowski for assisting with primary data collection; H. Russell, C. Evans, and B. Walter for assisting with data processing and compilation; and K. McWhinnie, S. Carell, J. Krasinski, R. Wilson, and J. Fischer for moral support. This work was supported by an NSF-CAREER grant to T.R.R. (IOS-1651888).

AUTHOR CONTRIBUTIONS

Conceptualization: T.R., R.M., and J.S. Methodology: T.R., R.M., and J.S. Analysis: R.M., T.R., and J.S.

Respirometry device construction: J.S. and R.M. Writing: R.M., J.S., and T.R. Funding acquisition: T.R.

COMPETING INTERESTS

The authors declare no competing or financial interests.

DATA AVAILABILITY STATEMENT

Data will be deposited to GitHub repository upon acceptance at www.github.com/jasonsckrabulis/mcwhinnie_etal_respirometry

REFERENCES

- Altman KA, Paull SH, Johnson TJ *et al.* (2016). Host and parasite thermal acclimation responses depend on the stage of infection. *Journal of Animal Ecology* **85**, 1014–24.
- Berger L, Speare R, Daszak P *et al.* (1998). Chytridiomycosis causes amphibian mortality associated with population declines in the rain forests of Australia and Central America. *PNAS* **95**, 9031–6.
- Bilyk KT, DeVries AL (2011). Heat tolerance and its plasticity in Antarctic fishes. *Comparative Biochemistry and Physiology* **158**, 382–90.
- Boutilier RG (1984). Characterization of the intermittent breathing pattern in *Xenopus laevis*. *Journal of Experimental Biology* **110**, 291–309.
- Brett SS, Shelton G. (1979). Ventilatory mechanisms of the amphibian, *Xenopus laevis*; the role of the buccal force pump. *Journal of Experimental Biology* **80**, 251–69.
- Brown JH, Gillooly JF, Allen AP *et al.* (2004). Toward a metabolic theory of ecology. *Ecology* **85**, 1771–89.
- Burggren W (2018). Developmental phenotypic plasticity helps bridge stochastic weather events associated with climate change. *Journal of Experimental Biology* **221**, jeb161984.
- Denny MW, Dowd WW (2012). Biophysics, environmental stochasticity, and the evolution of thermal safety margins in intertidal limpets. *Journal of Experimental Biology* **215**, 934–47.
- Dell AI, Pawar S, Savage VM (2011). Systematic variation in the temperature dependence of physiological ecological traits. *PNAS* **108**, 10591–6.
- Donelson JM, Salinas S, Munday PL, Shama LN (2018). Transgenerational plasticity and climate change experiments: Where do we go from here?. *Global Change Biology* **24**, 13–34.

- Emilio MG, Shelton G (1974). Gas exchange and its effect on blood gas exchange in the amphibian, *Xenopus laevis*. *Journal of Experimental Biology* **60**, 567–79.
- Emilio MG, Shelton G (1980). Carbon dioxide exchange and its effects on pH and bicarbonate equilibria in the blood of the amphibian, *Xenopus laevis*. *Journal of Experimental Biology* **85**, 253–62.
- Feder ME (1983). Responses to acute hypoxia in larvae of the frog *Rana berlandieri*. *Journal of Experimental Biology* **104**, 79–95.
- Feder ME, Wassersug RJ (1984). Aerial versus aquatic oxygen consumption in larvae of the clawed frog, *Xenopus laevis. Journal of Experimental Biology* **108**, 231–45.
- Fonseca EM, da Silva GS, Fernandes M *et al.* (2012). The breathing pattern and the ventilatory response to aquatic and aerial hypoxia and hypercarbia in the frog *Pipa carvalhoi. Comparative Biochemistry and Physiology Part A: Molecular, Integrative Physiology* **162**, 281–7.
- Gillooly JF, Allen AP, Savage VM *et al.* (2006). Response to Clarke and Fraser: Effects of temperature on metabolic rate. *Functional Ecology* **20**, 400–4.
- Gillooly JF, Brown JH, West GB *et al.* (2001). Effects of size and temperature on metabolic rate. *Science* **293**, 2248–51.
- Gillooly JF, Gomez JP, Mavrodiev EV *et al.* (2016). Body mass scaling of passive oxygen diffusion in endotherms and ectotherms. *PNAS* **113**, 5340–5.
- Glass ML, Boutilier RG, Heisler N (1983). Ventilatory control of arterial P_{O2} in the turtle *Chrysemys picta bellii*: Effects of temperature and hypoxia. *Journal of Comparative Physiology* **151**, 145–53.
- Glazier DS (2005). Beyond the '3/4-power law': Variation in the intra- and interspecific scaling of metabolic rate in animals. *Biological Reviews* **80**, 611–62.
- Glazier DS (2010). A unifying explanation for diverse metabolic scaling in animals and plants. *Biological Review* **85**, 111–38.
- Glazier DS (2014a). Metabolic scaling in complex living systems. *Systems* **2**, 451–40.
- Glazier DS (2014b). Scaling of metabolic Scaling within physical limits. *Systems* **2**, 425–50.
- Gottlieb G, Jackson DC (1976). Importance of pulmonary ventilation in respiratory control of the bullfrog. *American Journal of Physiology Legacy Content* **230**, 608–13.
- Green SL (2010). *The Laboratory* Xenopus *sp.*. CRC Press, Boca Raton, FL.

- Greven H, Zanger K, Schwinger G (1995). Mechanical properties of the skin of *Xenopus laevis* (Anura, Amphibia). *Journal of Morphology* **224**, 15–22.
- Halsey LG, Butler PJ, Blackburn TM (2006). A phylogenetic analysis of the allometry of diving. *The American Naturalist* **167**, 276–87.
- Hastings D, Burggren W (1995). Developmental changes in oxygen consumption regulation in larvae of the south African clawed frog *Xenopus laevis*. *Journal of Experimental Biology* **198**, 2465–75.
- Hedrick MS, Hillman SS, Drewes RC, Withers PC (2011). Pulmonary compliance and lung volume varies with ecomorphology in anuran amphibians: implications for ventilatory-assisted lymph flux. *Journal of Experimental Biology* **214**, 3279–85.
- Hillman SS, Withers PC (1979). An analysis of respiratory surface area as a limit to activity metabolism in anurans. *Canadian Journal of Zoology* **57**, 2100–5.
- Hillman SS, Withers PC (1981). Aerobic contributions to sustained activity metabolism in *Xenopus laevis*. Comparative Biochemistry and Physiology Part A: Physiology 69, 605–6.
- Hutchison VH, Miller K (1979). Aerobic and anaerobic contributions to sustained activity in *Xenopus laevis*. *Respiratory physiology* **38**, 93–103.
- Hutchison VH, Whitford WG, Kohl M (1968). Relation of body size and surface area to gas exchange in anurans. *Physiological Zoology* **41**, 65–85.
- Keeling RF, Garcia HE (2002). The change in oceanic O₂ inventory associated with recent global warming. *PNAS* **99**, 7848–53.
- Killen SS, Atkinson D, Glazier DS (2010). The intraspecific scaling of metabolic rate with body mass in fishes depends on lifestyle and temperature. *Ecology Letters* **13**, 184–93.
- Leroi AM, Bennett AF, Lenski RE (1994). Temperature acclimation and competitive fitness: an experimental test of the beneficial acclimation assumption. *PNAS* **91**, 1917–21.
- Morash AJ, Neufeld C, MacCormick TJ, Currie S (2018). The importance of incorporating natural thermal variation when evaluating physiological performance in wild species. *Journal of Experimental Biology* **221**, jeb164673.
- Nagano Y, Ode KL (2014). Temperature-independent energy expenditure in early development of the African clawed frog, *Xenopus laevis*. *Physical biology* 11, 046008.

- Ohlberger J, Mehner T, Holker F (2012). Intraspecific temperature dependence on the scaling of metabolic rate with body mass in fishes and its ecological implications. *Oikos* **121**, 245–51.
- Padilla P, Ducret V, Bonneaud C *et al.* (2019). Acclimation temperature effects on locomotor traits in adult aquatic anurans (*X. tropicalis* and *X. laevis*) from different latitudes: possible implications for climate change. *Conservation physiology* 7, coz019.
- Patterson MR (1992). A mass transfer explanation of metabolic scaling relations in some aquatic invertebrates and algae. *Science* **255**, 1421–3.
- R Core Team (2018). R: A Language and Environment for Statistical Computing. R Foundation for Statistical Computing, Vienna, Austria. Available from URL: https://www.R-project.org/
- Raffel TR, Romansic JM, Halstead NT *et al.* (2013). Disease and thermal acclimation in a more variable and unpredictable climate. *Nature Climate Change* **3**, 146.
- Rohr JR, Raffel TR, Blaustein AR *et al.* (2013). Using physiology to understand climate-driven changes in disease and their implications for conservation. *Conservation and Physiology* **1**, cot022.
- Rubner M (1883). Ueber den einfluss der korpergrosse auf stoffund kaftwechsel. *Zeitschrift fur Biologie* **19**, 535–62.
- Savage VM, Allen AP, Brown JH *et al.* (2007). Scaling of number, size, and metabolic rate of cells with body size in mammals. *PNAS* **104**, 4718–23.
- Savage VM, Deeds EJ, Fontana W (2008). Sizing up allometric scaling theory. *PLoS Computational Biology* 4, e1000171.
- Schreer JF, Kovacs KM (1997). Allometry of diving capacity in air-breathing vertebrates. *Canadian Journal of Zoology* **75**, 339–58.
- Seebacher F, Tallis JA, James RS (2014). The cost of muscle power production: muscle oxygen consumption per unit work increases at low temperatures in *Xenopus laevis*. *Journal of Experimental Biology* **217**, 1940–5.
- Seymour RS (1973). Physiological correlates of forced activity and burrowing in the spadefoot toad, *Scaphiopus hammondii*. *Copeia* **1973**, 103–15.
- Shannon P, Kramer DL (1988). Water depth alters respiratory behavior of *Xenopus laevis*. *Journal of Experimental Biology* **137**, 597–602.
- Skerratt LF, Berger L, Speare R *et al.* (2007). Spread of chytridiomycosis has caused the rapid global decline and extinction of frogs. *EcoHealth* **4**, 125–34.

- Stuart SN, Chanson JS, Cox NA *et al.* (2004). Status and trends of amphibian declines and extinctions worldwide. *Science* **306**, 1783–6.
- Tattersall GJ, Currie S, LeBlanc DM (2013). Pulmonary and cutaneous O₂ gas exchange: A student laboratory exercise in the frog. *Advances in Physiology Education* **37**, 97–105.
- Tsugawa K (1982). Effects of cold acclimation on the standard metabolic rate and osmotic fragility of erythrocytes in an aquatic anura, *Xenopus laevis*. *Comparative Biochemistry and Physiology Part A: Physiology* 73, 431–6.
- VanBuren CS, Norman DB, Frobisch NB (2018). Examining the relationship between sexual dimorphism in skin anatomy and body size in the white-lipped tree frog. *Litoria infrafrenata* (Anura: Hylidae). *Zoological Journal of the Linnean Society* **186**, 491–500.
- West GB, Brown JH, Enquist BJ (1999). The fourth dimension of life: Fractal geometry and allometric scaling of organisms. *Science* **284**, 1677–9.
- White CR, Seymour RS (2003). Mammalian basal metabolic rate is proportional to body mass^{2/3}. *PNAS* **100**, 4046–9.
- Whitford WG (1973). The effects of temperature on respiration in the Amphibia. *American Zoologist* **13**, 505–12.
- Withers PC, Hedrick MS, Drewes RC, Hillman SS (2014). Pulmonary compliance and lung volume are related to terrestriality in anuran amphibians. *Physiological and Biochemical Zoology* **87**, 374–83.
- Wilson RS, Franklin CE (2002). Testing the beneficial acclimation hypothesis. *TRENDS in Ecology, Evolution* **17**, 66–70.
- Wilson RS, James RS, Johnston IA (2000). Thermal acclimation of locomotor performance in tadpoles and adults of the aquatic frog *Xenopus laevis*. *Journal of Comparative Physiology B* **170**, 117–24.

SUPPLEMENTARY MATERIALS

Additional supporting information may be found online in the Supporting Information section at the end of the article.

- **Table S1** Thermal performance models testing the effects of acclimation temperature (AccTemp) and inverse performance temperature (PerfTemp⁻¹) for the primary controlled-temperature experiment at individual time points.
- **Table S2** Comparison of estimates for key MTE parameters with and without additional measurements from smaller post-experiment frogs.
- **Table S3** Breath bout mass- and volume-scaling coefficients ("b") for the primary controlled-temperature experiment.
- **Table S4** Grouped performance temperatures ("Cool" temperatures [8, 11, 14, & 17°C]; "Warm" temperatures [20, 23, 26, & 29°C]) for comparison of mass- and volume-scaling exponents in the breath bout dataset from the primary controlled-temperature experiment.
- **Table S5** Average breaths per minute (bpm) in the primary controlled-temperature experiment for frogs in different mass groups and performance temperatures, for comparison with previously published data by Boutilier (1984).
- **Figure S1** Respirometry device schematic and photos. (a) Schematic of Adafruit Pro Trinket microcontroller and electronic components.
- **Figure S2** Process of baseline-correcting time series data for oxygen percentage (a,b) and air flow rate (c,d) for a single representative breath bout.
- **Figure S3** Thermal performance curves across all time points in the primary controlled-temperature experiment.
- **Figure S4** Thermal performance curves for all metabolic proxies for one, four, and eight days post-acclimation in the primary controlled-temperature experiment.
- **Figure S5** Characteristic breathing patterns of *X. laevis* observed in this study.
- **Figure S6** Proportion cutaneous respiration as a function of log-transformed frog mass, showing all measurements including the eight smaller frogs measured after the primary controlled-temperature experiment was completed.
- **Figure S7** Dissolved oxygen availability and proportion of respiration performed cutaneously as functions of temperature in the primary controlled-temperature experiment.

Cite this article as:

McWhinnie RB, Sckrabulis JP, Raffel TR (2021). Temperature and mass scaling affect cutaneous and pulmonary respiratory performance in a diving frog. *Integrative Zoology* **00**, 1–17.

Supplementary Information – Methods

2 Constructing an Arduino-based digital device for flow-through respirometry

We developed a low-cost, microcontroller-driven system to measure oxygen concentration and airflow rate for use in a setup described by Boutilier (1984). Using available parts and sensors, we were able to keep the cost for a single unit under \$200 with a footprint smaller than a mousepad, with components housed inside a rectangular project box (12.5 × 9 × 4 cm). This allowed us to set up an individual flow-through sensor unit for each of the twelve incubators used in the performance-temperature measurements. Devices were designed to record and save measurements to an external memory card at an average of 82 readings per second over the time frame of each respirometry measurement. Each unit was attached to a respiratory chamber setup that allowed the frog to choose between breathing air or diving (Fig. 1; described below), based on the classic funnel-based design described by Boutilier (1984).

We designed the unit to use a microcontroller based on the Arduino open-source prototyping platform, due to its relative ease-of-use for people with little programming and electronics experience (www.arduino.cc). Since its original release, an enormous knowledge base has accumulated for hardware schematics, code examples, and software applications. Due to its open-source nature, other companies have taken the original Arduino microcontroller board and tailored it to their particular needs.

Specifically, the Adafruit Pro Trinket product line (Adafruit Industries, New York, New York, USA) has a reduced number of input and output pins, dramatically reducing its footprint and cost. Our system required fast processing and 5V sensors, so we used the Pro Trinket 5v 16MHz model.

Electronic components

To measure air flow rate, we used the ZephyrTM analog gas flow sensor package (Honeywell, Charlotte, North Carolina, USA). These sensors directly measure the change in resistance of temperature-sensitive resistors influenced by the air flow rate. The ZephyrTM line was designed for medical and industrial use and has a fast response time, customizable packages, and linear output for easier integration into the user's application. Oxygen concentration was measured as a volumetric percentage using the Seeed Grove O₂ sensor package designed for the Arduino platform (Seeed Studio, Shenzhen, China). This module uses the ME2 oxygen gas sensor, designed for oxygen detection in enclosed areas (i.e., mines). The ME2 sensor detects gas concentration by measuring the change in current based on the electrochemical reaction of the gas on a heated electrode. Because the sensor was designed for open applications, we custom-built a flow-through air chamber by modifying and sealing a plastic coin case,

which fit over the interface surface to ensure that air flowing through the system was the only air accessed by the sensor.

Device operation

This system was designed to be battery-powered or powered via an appropriate DC power supply. Once the user supplies power to the device, it enters a 'standby' phase waiting for the user to flip the switch. Once the switch is detected, it enters a 'warm-up' phase where voltage is provided to the ME2 oxygen sensor for an equilibration period of 20 minutes. The device then enters the 'data collection' phase, during which it records the initial time of data collection and starts logging flow rate, oxygen concentration, and the time (in milliseconds) since power was supplied. After the data collection period, the user flips the switch to enter 'standby' and stops supplying voltage to the sensors, ending data collection and writing the datafile to a microSD memory card. Additional data collection periods can be obtained by continuously flipping the switch as needed until the device is powered off. A complete pictorial schematic of the respirometer is depicted in the main text as Figure S1.

Operating code

- Full code and schematics are available at
- 47 <u>www.github.com/jasonsckrabulis/mcwhinnie_etal_respirometry</u>.

Respirometry setup – detailed methods

Each frog was given a bottle height between 9–12 cm, based on the frogs' ability to easily surface for breathing. All total water volumes ranged between 559 and 824 mL for 9 and 12 cm bottles, respectively. A total of 175 holes (approximately one millimeter in diameter) were punctured throughout the funnel to allow for a standardized amount of oxygen diffusion between water inside and outside the funnel. These holes are necessary for water displacement when each animal breathes air in and expands, otherwise changes in flow rate will not be detectable due to equal volumes of water and air changing simultaneously within the funnel. Sculpting clay was used to form a ring around the perimeter inside the bottom of the cup to hold the bottle in place for constant height and to reduce unwanted background noise from jostling of the bottle from animal movement. Deli cups were filled to a fixed location on the bottle for each bottle height to ensure consistently accurate water volumes for all setups. Custom foam sheets were designed to act as oxygen diffusion blockers and cover all water surface area to effectively prohibit diffusion between atmospheric and aquatic dissolved oxygen. Figure 1 depicts the complete respiration setup for each frog, including the incubator array and individual deli cup setup for each frog. An air pump supplied a constant air flow rate for up to four frogs simultaneously for each row of incubators, for a total

of three rows, or a total of 12 incubators. Air flow traveled from the pump through a series of two quartsized mason jars to reduce unwanted variations in flow rate deemed 'noise' in flow rate measurements. Air flow then travelled into the incubator and to the air chamber for the frog to respire. Once the air passes through the incubator, flow rate and % O₂ measurements are taken by the respirometry device before being released back into the experimental room.

Quantifying cutaneous oxygen consumption

Cutaneous oxygen uptake (COU) was quantified by measuring changes in dissolved oxygen (DOppm) concentrations (mg O₂ L⁻¹) during the animal's respirometry trial, using a ProOBOD Optical BOD Probe (YSI, Yellow Springs, Ohio, USA). For each measurement, the mass of oxygen available at the start of the performance measurement (SDO) for a given volume of water (V_W) was calculated by multiplying each DOppm measurement by water volume. For example, the starting value for oxygen mass in water was calculated according to Equation 1.

$$SDO = DO_{ppm} \cdot V_W \tag{1}$$

A single initial dissolved oxygen measurement for each animal was obtained, taking the measurement just prior to adding the animal to the container. However, due to the complexity of the respirometry apparatus with each animal held within a perforated funnel, it was necessary to obtain separate endpoint measurements (DO_{ppm} and V_W) from both inside the funnel (FDO_{Int}) and outside the funnel (FDO_{Ext}) for each animal. Once all three measurements were transformed to volume-corrected units of mg O_2 using Equation 1, total oxygen consumption and rate (I_C) for each trial length in hours (TL_{hr}^{-1}) was then calculated according to Equations 2 and 3.

$$COU = SDO - (FDO_{Int} + FDO_{Ext})$$
 (2)

$$I_C = COU \cdot TL_{hr}^{-1} \tag{3}$$

Quantifying pulmonary oxygen consumption

The first step in data processing was to establish a baseline level for a flow rate and percent O₂ (%O₂), as defined by the values for each of these parameters when frogs were not breathing. When plotted as a time series, these breath bouts are visually distinguishable from the gaps between breaths, making it possible to select representative baseline data points between breath bouts and use it to establish a continuous running baseline through the entire time series. We used the *fhs* function from the *gatepoints* package to freehand select representative data points for each baseline, excluding data points more than 5 mL min⁻¹ or 0.1 % away from the visually apparent baseline for each flow or O₂ dataset, respectively

(Fig. S2A, C). Once this was done, the *na.fill* function from the *zoo* package was used to fill "NA"s from the selected baseline dataset based on the surrounding data. To finalize baseline correction, a cubic smoothing spline was fit to each baseline dataset to generate a continuous baseline function (smooth.spline from the base package). The spline fit was then subtracted from the original (raw) dataset to generate a baseline-corrected (e.g., BCO_i and $FlowBC_i$) data series through time (Δt_i) centered around zero (POM; e.g., Fig. S2B, D). Following baseline correction, breath bout volumes and total oxygen consumption were calculated by multiplying the change in flow rate or percent oxygen from the baseline against the time frame for each specific measurement. A pre-established approach was used for the exclusion of all non-negative oxygen values (above baseline) from analysis. These values yield the volume of flow or percent oxygen for each reading with sums being added for both positive and negative values to determine respective values for the entire measurement. Standard values for volumetric percent of oxygen in air $(O2STP_V^{-1})$, mass percentages of oxygen in air $(O2STP_M)$, and corrected flow rate (F_i) were used and local air density (LAD) were calculated using temperature (T_{rm}) and elevation (in atmospheres; AP) of measurement location relative to standard temperature and pressure conditions (FlowSTP_i and T_{STP}). Trial lengths were also calculated in minutes (TL_{min}) or seconds (TL_{sec}). The pulmonary oxygen consumption rate (POU) over the measurement period was then calculated for each respirometry trial (or individual breath bout; see below) and metabolic rates for pulmonary (I_P) and total (I_T) oxygen consumption were calculated, using the following series of stoichiometric equations (4-8).

94

95

96

97

98

99

100

101

102

103104

105

106107

108

109

110

111

117

118

119

120

121

122

123

$$F_i = \frac{FlowSTP_i \cdot T_{rm}}{T_{STP} \cdot AP} \tag{4}$$

113
$$POM = \sum (BCO_i \cdot \Delta t_i) = \sum \left(\%O_2 \cdot \frac{1}{100} \cdot \Delta t_i \right)$$
 (5)

$$POU = POM \cdot F_i \cdot LAD \cdot O2STP_M \cdot O2STP_V^{-1} \cdot \frac{1000 \, mg}{1 \, g} \cdot \frac{TL_{min}}{TL_{sec}}$$
 (6)

$$I_P = POU \cdot TL_{hr}^{-1} \tag{7}$$

$$I_T = (COU + POU) \cdot TL_{hr}^{-1} \tag{8}$$

Pulmonary measurements (i.e., ventilation frequency and pulmonary O₂ consumption) were omitted from analyses when a frog breathed fewer than three times during a full session. We omitted eight datapoints for frogs with zero breaths, and two for frogs with 1–2 breaths.

Quantifying oxygen consumption and breath volumes for individual breaths

To quantify the relationship between breath volume and oxygen consumption, data were collected for isolated breath bouts within each zero-day measurement and calculated corresponding breath volumes and oxygen consumption. A 'breath bout' is here defined as a distinct period of breathing activity,

encompassing one or more individual breaths, that is sufficiently separated from other breaths so that both flow rate and percent oxygen could completely return to baseline levels in between measurements. Only pulmonary metabolic proxies were examined for the breath bout dataset, because cutaneous respiration was unable to be calculated for abbreviated time periods within the respirometry trial. Sudden animal movements sometimes led to signal noise in the flow rate data, which could reduce the accuracy of breath volume measurements, so for this analysis we purposefully selected "clean" breath bouts without excess signal noise (e.g., Fig. S2; Fig. S5) from respirometry sessions at the zero-day time point. Fewer than three breath bouts were quantified for eleven sessions due to absence of pulmonary respiration (three frogs), lack of 'clean' windows containing isolated breath bouts (seven frogs), or technical problems leading to flow rates too low to detect individual breath bouts (one frog). Total breath volume for each breath bout was calculated from the baseline-corrected flow rate data, and then divided by number of breaths to generate the average breath volume (V_{breath}) as shown in Equation 9.

$$V_{breath} = \frac{1}{\#Breaths} \times \sum |FlowBC_i \times \Delta t_i| \times \frac{TL_{min}}{TL_{sec}}$$
 (9)

We also divided total oxygen uptake per breath bout by the number of breaths taken, and then averaged these values from up to three breath bouts per trial to generate mean pulmonary oxygen uptake and V_{breath} for each measurement period.

Experimental design – supporting details

During the acclimation period, frogs were housed in custom-built temperature-controlled incubators constructed according to Raffel et al. (2013) but modified to increase the internal dimensions (38 cm long × 24 cm wide × 13 cm height) and place heating elements on the walls instead of the floor. Each acclimation incubator contained up to two frogs in a total of 12 incubators, singly housed in individual 1 L deli cups. Frogs were assigned to individual incubators, constrained to ensure animals in the same acclimation incubator would be tested at different performance temperatures. Animals were checked and rotated daily to minimize potential effects of within-incubator temperature variation. All animals were fed California blackworms (*Lumbriculus variegatus*; Müller, 1774) *ad libitum* and a full water change was performed at least twice weekly, depending on water quality. Animals were not intentionally fasted prior to respirometry measurements, but we waited till after measurements were taken before feeding them on respirometry days.

We obtained one respiratory measurement per frog per day, except for the zero-day time point. To maximize the likelihood of detecting thermal acclimation effects on day zero, we measured respiratory performance for each animal at two different temperatures on this day, completing both measurements

within a six-hour time frame. Following each respirometry measurement, each animal was maintained at their most recently measured performance temperature until the next respirometry measurement, using a separate array of performance-period incubators (same construction as the acclimation-period incubators). HOBO loggers (Onset, Bourne, MA) were placed within incubators to ensure proper temperature was maintained throughout acclimation and performance periods. The average temperature of all acclimation and performance incubators throughout the experiment was within 0.6 °C of the target temperature, so the target temperature was used for all subsequent analyses.

Detailed statistical methods

155

156

157

158159

160

161

162

163

164165

166

167

168

169

170

171

172

173174

175

176177

178

179

180

181

182

183

184

185

186

We incorporated random effects into all linear mixed-effects models, to ensure we tested for statistical significance and calculated 95% confidence intervals using the proper level of replication for each explanatory variable. We used the function confint from the base package to generate 95% Wald confidence intervals for parameters of interest (E_A and b estimates). To ensure that temperature treatments were properly replicated at the incubator level (see Raffel et al., 2013), we tracked which incubator was used during each acclimation period or respirometry measurement and included random effects of acclimation and performance incubator in each statistical model. We also accounted for the potential effect of having multiple measurements of a given frog by including frog identification as a random effect, which was nested within acclimation incubator for each experiment. The resulting error structure for each model was coded as: (1|AccInc/FrogID) + (1|PerfInc). Effective sample sizes reported in the figure legends indicate the number of replication units for each predictor variable, each of which was assessed at a different level of nested random effects. Mass effects had about twice the number of replication units as the number of individual frogs, because the mass of each frog changed between experiment 1 and experiment 2. The function Anova from the car package was used to calculate type-II sums of squares with F-values, using Kenward-Rogers degrees of freedom (which can generate noninteger values).

Predictor coefficients and standard errors were taken from models with marginal terms and interactions removed, to ensure they could validly be used to interpret main effect directionalities and to estimate scaling exponents. All final models were chosen using backwards selection, removing terms with P-values > 0.1, unless otherwise noted. We also tested for quadratic effects of acclimation and performance temperature to detect possible curvilinear effects on performance for overall, through-time, and breath bout models. However, all four respiratory proxies of metabolic rate increased linearly with inverse temperature (no significant quadratic effects of inverse performance temperature for any metabolic proxy at any time point), so quadratic effects of performance temperature were removed from

a	ll final models. The acclimation temperature variable was centered around zero (i.e., subtracting the
n	nean acclimation temperature) to ensure linear effects of acclimation temperature would remain
iı	nterpretable in a polynomial regression context.

SUPPLEMENTARY MATERIALS

Table S1 Thermal performance models testing the effects of acclimation temperature (AccTemp) and inverse performance temperature (PerfTemp⁻¹) for the primary controlled-temperature experiment at individual time points. Statistical tests are based on linear mixed effects regression with the same random-effects structure as the Table 1 models, using F-tests with type II sums of squares and Kenward-Rogers d.f. All models initially included a quadratic effect of acclimation temperature and both linear (AccTemp \times PerfTemp⁻¹) and non-linear (AccTemp² \times PerfTemp⁻¹) interactions for comparison with the models presented in Table 1, but were simplified by backward selection to remove non-significant interactions (P > 0.05). Quadratic effects of acclimation temperature (AccTemp²) were retained in models for total and cutaneous O₂ consumption, to explore changes in this effect through time that might have driven the significant AccTemp² \times Time interactions reported in Table 1. PerfTemp⁻¹ exponents were multiplied by –k to generate E_A exponents for comparison with other analyses.

Response	Day	Predictor	Coef ± SE	F	D.f.	P
Total O ₂	+0	PerfTemp ⁻¹	0.475 ± 0.053	66.5	1, 56.5	< 0.001
		AccTemp	0.001 ± 0.008	0.0	1, 8.5	0.883
		AccTemp ²	-0.003 ± 0.001	3.8	1, 7.9	0.088
		ln Mass	0.456 ± 0.152	7.7	1, 33.5	0.009
	+1	PerfTemp ⁻¹	0.545 ± 0.075	38.8	1, 24.0	< 0.001
		AccTemp	0.001 ± 0.009	0.0	1, 11.9	0.865
		AccTemp ²	$4.403 \times 10^{-4} \pm 0.002$	0.1	1, 6.3	0.816
		ln Mass	0.534 ± 0.178	7.9	1, 24.7	0.009
	+4	PerfTemp ⁻¹	0.428 ± 0.070	28.1	1, 22.2	< 0.001
		AccTemp	0.001 ± 0.007	0.0	1, 4.0	0.839
		AccTemp ²	$6.757 \times 10^{-4} \pm 0.002$	0.1	1, 7.1	0.712
		ln Mass	0.203 ± 0.138	1.6	1, 21.1	0.216
	+8	PerfTemp ⁻¹	0.478 ± 0.076	31.9	1, 14.6	< 0.001
		AccTemp	0.013 ± 0.009	1.9	1, 6.4	0.213
		AccTemp ²	0.002 ± 0.002	1.4	1, 6.8	0.270
		In Mass	0.646 ± 0.179	10.4	1, 31.9	0.003
Cutaneous O ₂	+0	PerfTemp ⁻¹	0.313 ± 0.039	53.3	1, 61.9	< 0.001
		AccTemp	0.007 ± 0.006	1.0	1, 8.2	0.335
		AccTemp ²	-0.002 ± 0.001	2.2	1, 7.4	0.182
		ln Mass	0.300 ± 0.123	5.2	1, 35.5	0.028
	+1	PerfTemp ⁻¹	0.423 ± 0.045	67.0	1, 28.6	< 0.001
		AccTemp	0.014 ± 0.005	5.1	1, 11.4	0.045
		AccTemp ²	$-9.699 \times 10^{-4} \pm 9.350 \times 10^{-4}$	0.9	1, 7.2	0.369
		ln Mass	0.350 ± 0.102	10.5	1, 30.4	0.003
	+4	PerfTemp ⁻¹	0.173 ± 0.035	18.4	1, 22.3	< 0.001
		AccTemp	0.003 ± 0.004	0.8	1, 5.5	0.422
		AccTemp ²	$3.382 \times 10^{-4} \pm 8.280 \times 10^{-4}$	0.2	1, 7.5	0.685
		In Mass	0.175 ± 0.073	4.6	1, 27.4	0.040
	+8	PerfTemp ⁻¹	0.236 ± 0.048	19.9	1, 17.6	< 0.001
		AccTemp	0.007 ± 0.006	1.5	1, 7.3	0.265
		AccTemp ²	0.001 ± 0.001	1.4	1, 6.8	0.275

		In Mass	0.283 ± 0.119	4.7	1, 33.0	0.037
Pulmonary O ₂	+0	PerfTemp ⁻¹	0.720 ± 0.127	29.4	1, 72.1	< 0.001
		AccTemp	-0.009 ± 0.016	0.2	1, 9.5	0.693
		In Mass	0.802 ± 0.308	5.6	1, 32.8	0.022
	+1	PerfTemp ⁻¹	0.953 ± 0.224	15.3	1,22.1	< 0.001
		AccTemp	-0.009 ± 0.029	0.1	1, 13.5	0.772
		In Mass	0.825 ± 0.523	2.2	1, 24.2	0.148
	+4	PerfTemp ⁻¹	0.895 ± 0.141	35.6	1, 36.2	< 0.001
		AccTemp	$-2.545 \times 10^{-4} \pm 0.014$	0.0	1, 4.7	0.987
		In Mass	0.436 ± 0.294	1.7	1, 21.4	0.209
	+8	PerfTemp ⁻¹	0.930 ± 0.167	28.3	1, 35.8	< 0.001
		AccTemp	0.004 ± 0.020	0.0	1, 9.4	0.842
		In Mass	0.915 ± 0.377	4.9	1, 30.7	0.034
Ventilation frequency	+0	PerfTemp ⁻¹	0.210 ± 0.108	3.4	1, 72.8	0.068
1 3		AccTemp	-0.016 ± 0.015	1.0	1, 8.4	0.356
		In Mass	0.073 ± 0.305	0.0	1, 36.3	0.825
	+1	PerfTemp ⁻¹	0.278 ± 0.218	1.4	1, 29.6	0.245
		AccTemp	-0.064 ± 0.029	4.7	1, 11.3	0.053
		In Mass	-0.170 ± 0.423	0.1	1, 26.7	0.716
	+4	PerfTemp ⁻¹	0.677 ± 0.133	22.5	1, 22.7	< 0.001
		AccTemp	-0.002 ± 0.016	0.0	1, 8.4	0.887
		In Mass	-0.058 ± 0.336	0.0	1, 29.9	0.876
	+8	PerfTemp ⁻¹	0.030 ± 0.144	0.0	1, 36.0	0.845
		AccTemp	-0.016 ± 0.024	0.4	1, 9.1	0.523
		In Mass	-0.187 ± 0.347	0.2	1, 31.5	0.625

Table S2 Comparison of estimates for key MTE parameters with and without additional measurements from smaller post-experiment frogs. We re-ran linear mixed effects models with and without inclusion of these new measurements, to see how the expanded dataset influenced estimates of key MTE parameters. Models were simplified to remove fixed effects of acclimation temperature or time since acclimation, neither of which applied to the new measurements from smaller frogs. However, we retained the random-effects structure from the original mixed-effects models presented in Table 1. Regression coefficients for the effects of ln Mass provide direct estimates of mass-scaling coefficients (parameter "b"); PerfTemp⁻¹ coefficients were multiplied by –k for comparison with E_A estimates in other tables. Statistical tests were conducted using the Anova() function from the "car" package, which uses Kenward-Rogers degrees of freedom to compute F-statistics and p-values.

Response	Mass range	Predictor	Coef	95% CI	F	D.f.	P
	13.1–60.0 g	In Mass	0.444	0.219 - 0.668	13.5	1, 39.5	< 0.001
Total O		PerfTemp ⁻¹	0.457	0.401 - 0.512	250.9	1, 167.8	< 0.001
Total O ₂	1.9–60.0 g	In Mass	0.690	0.576 - 0.803	131.3	1, 13.4	< 0.001
		PerfTemp ⁻¹	0.444	0.389 - 0.499	242.0	1, 174.0	< 0.001
	13.1–60.0 g	In Mass	0.232	0.070 - 0.394	7.2	1, 39.2	0.011
Cutanaous O		PerfTemp ⁻¹	0.277	0.238 - 0.316	183.4	1, 185.8	< 0.001
Cutaneous O ₂	1.9–60.0 g	In Mass	0.472	0.372 - 0.571	77.9	1, 16.5	< 0.001
		PerfTemp ⁻¹	0.270	0.213 - 0.309	176.8	1, 189.6	< 0.001
	13.1–60.0 g	In Mass	0.791	0.349 - 1.233	11.1	1, 39.5	0.002
Dulmonomy O		PerfTemp ⁻¹	0.795	0.666 - 0.924	142.2	1, 161.5	< 0.001
Pulmonary O ₂	1.9–60.0 g	In Mass	1.565	1.311 -1.819	134.5	1, 16.1	< 0.001
	_	PerfTemp ⁻¹	0.770	0.640 -0.900	131.9	1, 164.3	< 0.001
	13.1–60.0 g	In Mass	0.214	-0.249 - 0.677	0.7	1, 39.8	0.395
Ventilation		PerfTemp ⁻¹	0.367	0.243 - 0.492	32.2	1, 165.4	< 0.001
frequency	1.9–60.0 g	In Mass	0.225	0.004 - 0.445	3.7	1, 13.4	0.077
		PerfTemp ⁻¹	0.373	0.250 - 0.496	34.3	1, 173.3	< 0.001

Table S3 Breath bout mass- and volume-scaling coefficients ("b") for the primary controlled-temperature experiment. Statistical tests are based on linear mixed effects regression, using F-tests with type II sums of squares and Kenward-Rogers d.f. Predictor coefficients were taken from models with marginal terms removed, to ensure they could be used to interpret main effect directionalities and to estimate b. Non-significant interaction terms were removed from models via backward selection (P > 0.05). Predictor coefficients were taken from models with marginal terms removed, to ensure they could be used to interpret main effect directionalities.

Response	Predictor	Coef ± SE	F	D.f.	P
ln O ₂ uptake	$ln V_{Breath}$	0.755 ± 0.131	27.2	1, 56.8	< 0.001
	AccTemp	-0.011 ± 0.011	0.8	1, 8.3	0.397
	PerfTemp	0.028 ± 0.012	5.5	1, 52.2	0.023
	In V _{Breath} * PerfTemp	-0.046 ± 0.018	5.7	1, 57.3	0.020
ln O ₂ uptake	In Mass	0.771 ± 0.262	8.4	1, 38.0	0.006
	AccTemp	-0.018 ± 0.014	1.4	1, 9.2	0.259
	PerfTemp	0.041 ± 0.014	7.4	1, 58.2	0.008
	In Mass * PerfTemp	-0.090 ± 0.037	5.0	1, 63. 3	0.028
ln V _{Breath}	ln Mass	0.946 ± 0.159	31.6	1, 37.8	< 0.001
	AccTemp	-0.011 ± 0.008	1.4	1, 10.0	0.261
	PerfTemp	0.014 ± 0.091	1.9	1, 57.0	0.173
In Ventilation frequency	ln Mass	0.265 ± 0.205	1.6	1, 37.5	0.213
	AccTemp	0.024 ± 0.009	5.8	1, 8.7	0.040
	PerfTemp	-0.015 ± 0.012	1.6	1, 56.3	0.213
	ln Mass * PerfTemp	0.120 ± 0.029	14.8	1, 60.5	< 0.001

Table S4 Grouped performance temperatures ("Cool" temperatures [8, 11, 14, & 17 °C]; "Warm" temperatures [20, 23, 26, & 29 °C]) for comparison of mass- and volume-scaling exponents in the breath bout dataset from the primary controlled-temperature experiment. Coefficients \pm SE represent both volume- and mass-scaling exponents, the latter of which is referred to as b in the main text.

Response	Temp range	Predictor	Coef ± SE	F	D.f.	P
O ₂ uptake	Cool	$ln \ V_{Breath}$	1.089 ± 0.150	36.3	1, 24.1	< 0.001
	Warm	$ln V_{Breath}$	0.460 ± 0.195	4.2	1, 32.3	0.050
O ₂ uptake	Cool	In Mass	1.435 ± 0.400	11.8	1, 24.6	0.002
	Warm	In Mass	0.381 ± 0.307	1.2	1, 23.1	0.280
V_{Breath}	Cool	In Mass	1.123 ± 0.243	18.4	1, 23.9	< 0.001
	Warm	In Mass	0.862 ± 0.209	13.5	1, 23.1	0.001
Ventilation frequency	Cool	In Mass	-0.695 ± 0.393	2.9	1, 25.1	0.099
	Warm	In Mass	0.710 ± 0.204	9.5	1, 21.2	0.006

Table S5 Average breaths per minute (bpm) in the primary controlled-temperature experiment for frogs in different mass groups and performance temperatures, for comparison with previously published data by Boutilier (1984). In general, frogs had faster breath rates when they had higher body masses and were measured at higher temperatures. The range of breath rates observed in this study were consistent with breath rates observed by Boutilier (1984) at 25 °C (0.77 \pm 0.17 bpm). Boutilier's measurement represents mean \pm SE.

		Performance temperature							
Mass range	8	11	14	17	20	23	26	29	
13.1–22.4 g	0.049	0.796	0.566	0.753	0.561	0.395	0.793	0.522	
22.6–29.6 g	0.361	0.724	0.573	0.651	0.858	0.919	0.879	1.292	
31.3–36.7 g	0.592	0.341	0.319	0.539	0.582	0.449	1.009	0.904	
37.5–60.0 g	0.513	0.290	0.525	0.608	0.928	1.119	1.023	1.424	

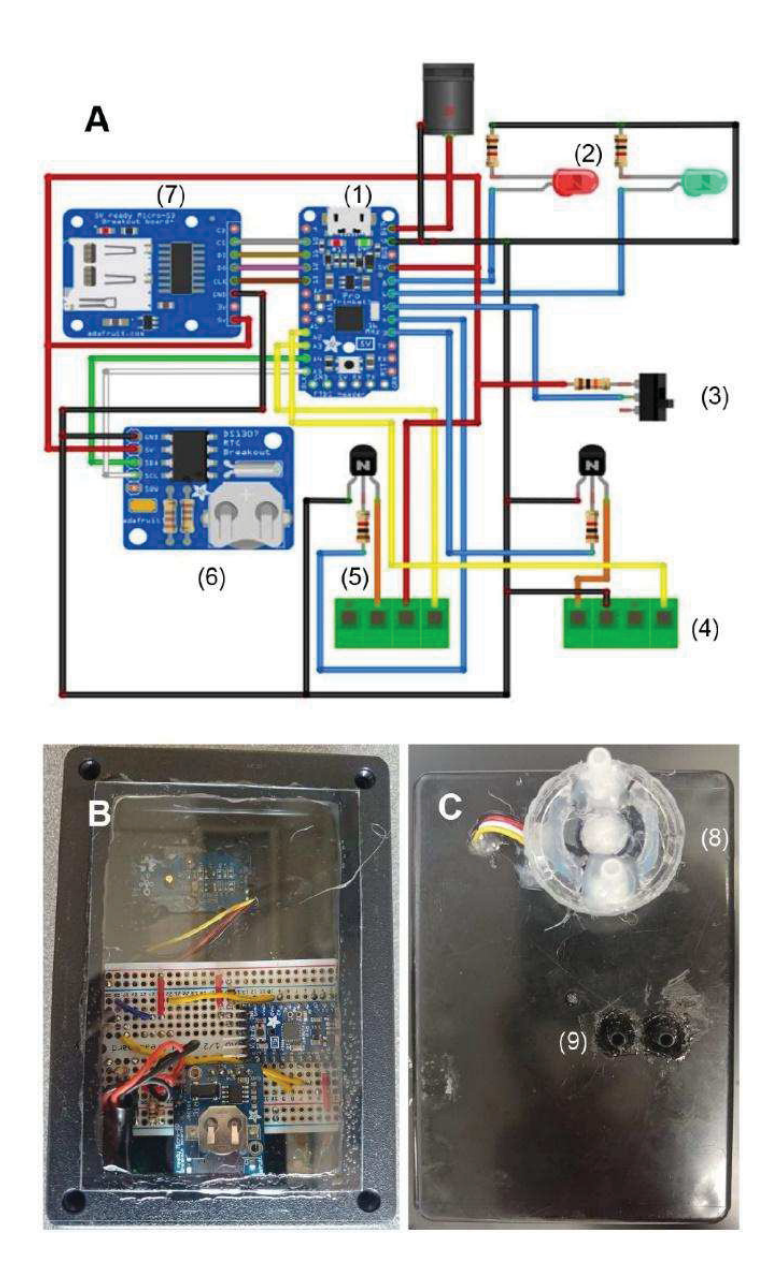


Figure S1 Respirometry device schematic and photos. A. Schematic of Adafruit Pro Trinket microcontroller and electronic components. Wire colors are based on standard electronics coding. Numbers indicate components: (1) Pro Trinket, (2) Power jack and indicator LEDs, (3) input switch, (4) Seeed Grove oxygen sensor, (5) Zephyr™ flow sensor, (6) Real-time clock module, and (7) microSD card module. (4) and (5) are depicted as generic connectors, but the right-most pin is "pin 1" of each module. Schematic generated in Fritzing (v0.9.3; www.fritzing.org) with Adafruit, Seeed Studio, and Sparkfun parts libraries. B. Front of a respirometry device, which has a clear cover to allow visualization of LED lights inside the box during measurements. C. Back of a respirometry device, showing (8) oxygen sensor covered by a modified plastic coin holder that channels air over the sensor and (9) airflow sensor ports.

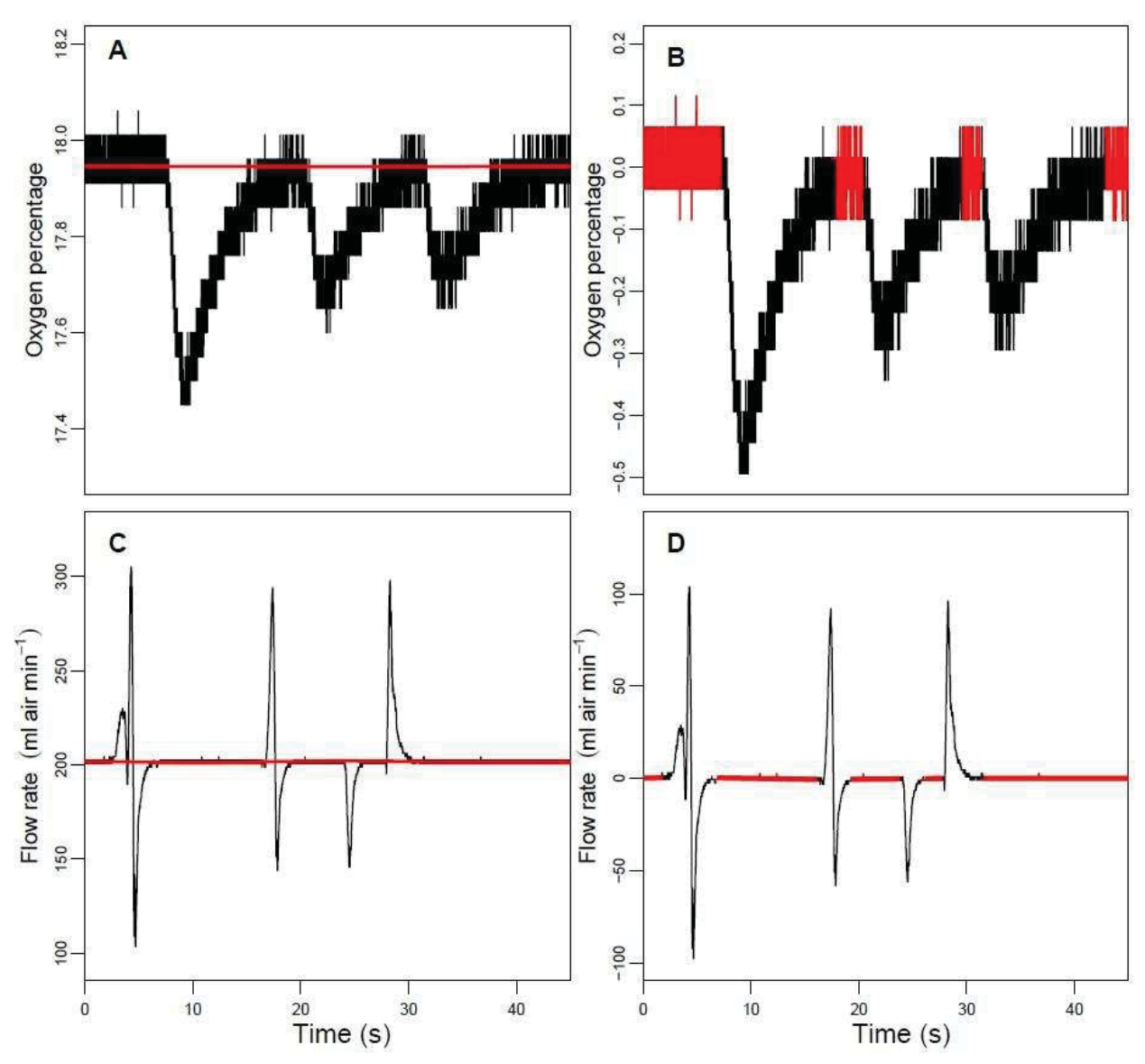


Figure S2 Process of baseline-correcting time series data for oxygen percentage (A, B) and air flow rate (C, D) for a single representative breath bout. The baseline itself (red curve in panels A & C) was generated by fitting a smoothing spline to the selected baseline data, and this baseline was then subtracted from the raw data to generate a baseline-corrected dataset. The smoothing spline fit (red line), representing the baseline, is superimposed over the raw data (black lines) in panels A & B. Data selected to represent the "baseline" (red lines) are superimposed over the raw data (black lines) in panels C & D. There is approximately a 3–5s delay between changes in flow rate and changes in oxygen percentage because of the time it takes the air from the frog to react with the oxygen sensor, whereas the change in air flow rate is instantaneously measured. In panels C and D, peaks in flow rate reflect exhalations and valleys reflect inhalations.

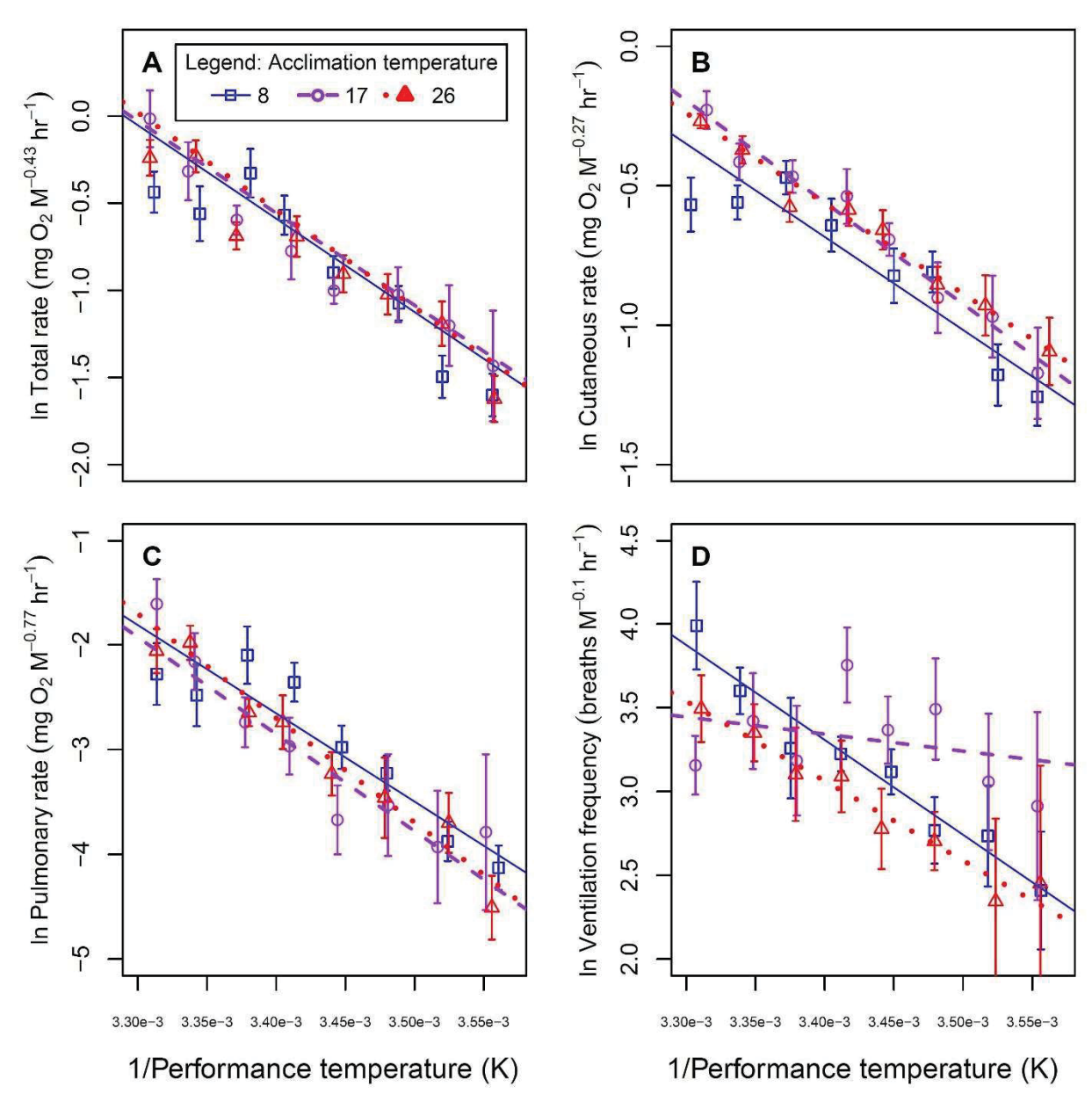


Figure S3 Thermal performance curves across all time points in the primary controlled-temperature experiment. (A) Total respiration (N=64.9). (B) Cutaneous respiration (N=62.6). (C) Pulmonary respiration (N=44.6). (D) Ventilation frequency (mass-scaled breaths per hour; N=52.8). All response variables were natural log transformed and scaled according to the observed mass scaling effects. Here, N indicates replication units for testing performance temperature effects in mixed-effects regression, which may be non-integer due to missing data points for some frogs. Error bars represent the standard error of each treatment group containing N > 1 replicates, and points were jittered using the "jitter" function in R to reduce visual overlap.

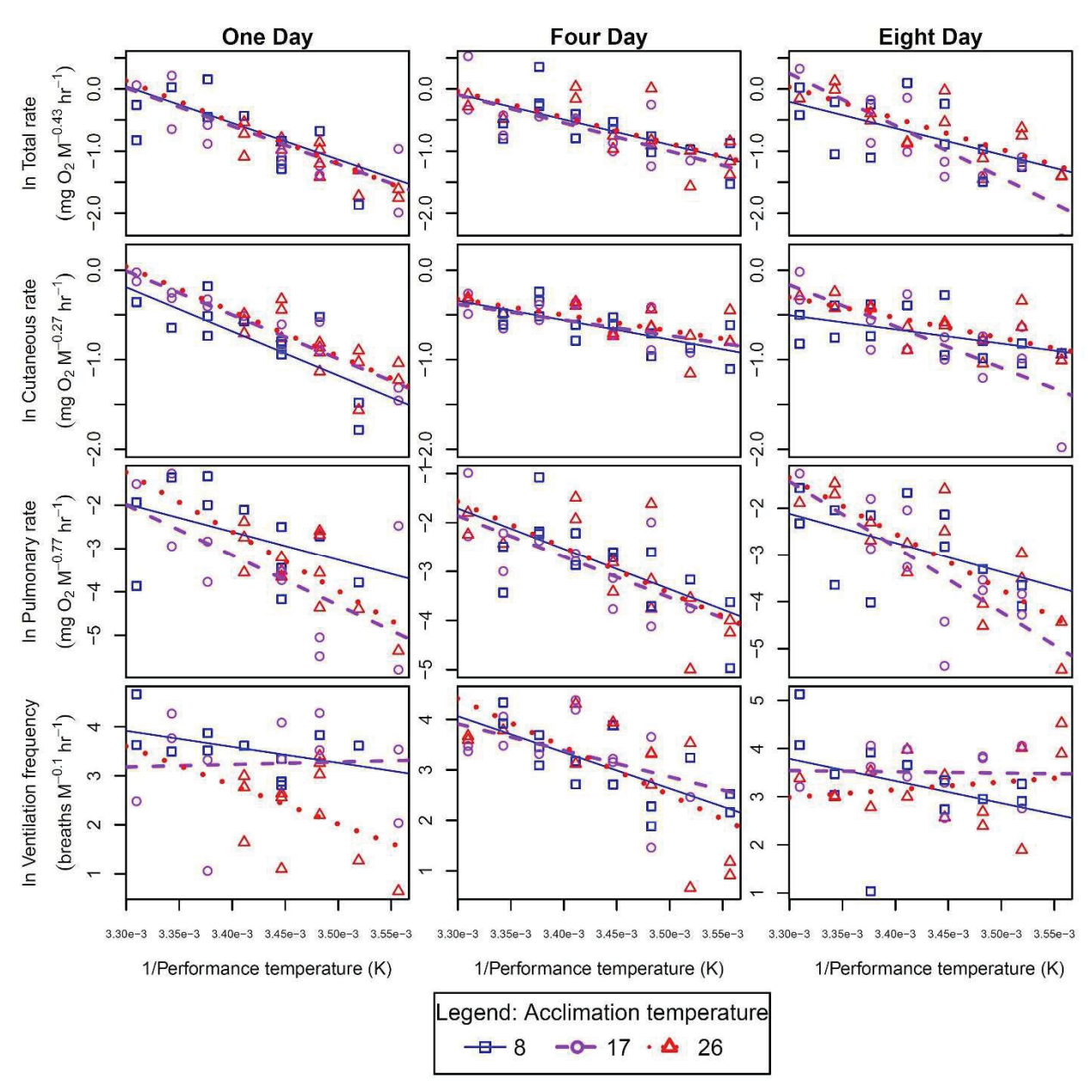


Figure S4 Thermal performance curves for all metabolic proxies for one, four, and eight days post-acclimation in the primary controlled-temperature experiment. Total O_2 consumption rate (N=33, 38, & 37 for days 1, 4, & 8, respectively), Cutaneous O_2 consumption rate (N=38, 39, & 39), Pulmonary O_2 consumption rate (N=31, 37 & 35), and Ventilation frequency (N=31, 37, & 35) are plotted as functions of inverse performance temperature (in Kelvin). All response variables were natural log transformed and scaled according to the observed mass scaling effects.

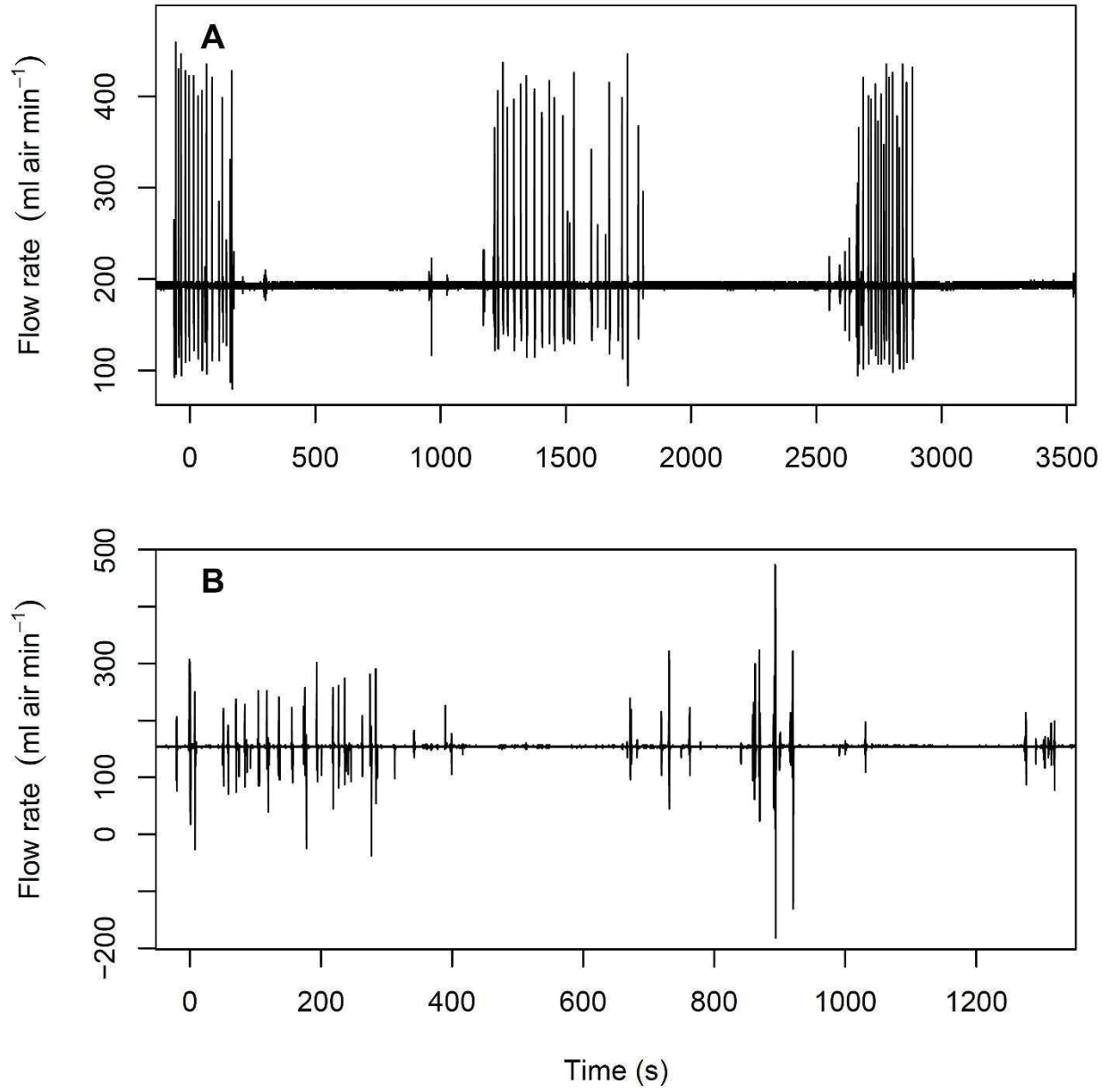


Figure S5 Characteristic breathing patterns of *X. laevis* observed in this study. (A) 'Burst' breathing pattern, in which frogs alternated between long periods without pulmonary respiration and shorter periods with many breaths in quick succession. (B) 'Bout' breathing pattern, in which frogs took regular or intermittent breaths throughout the measurement period. These patterns and more are described in greater detail by Boutilier (1984) and Brett and Shelton (1978).

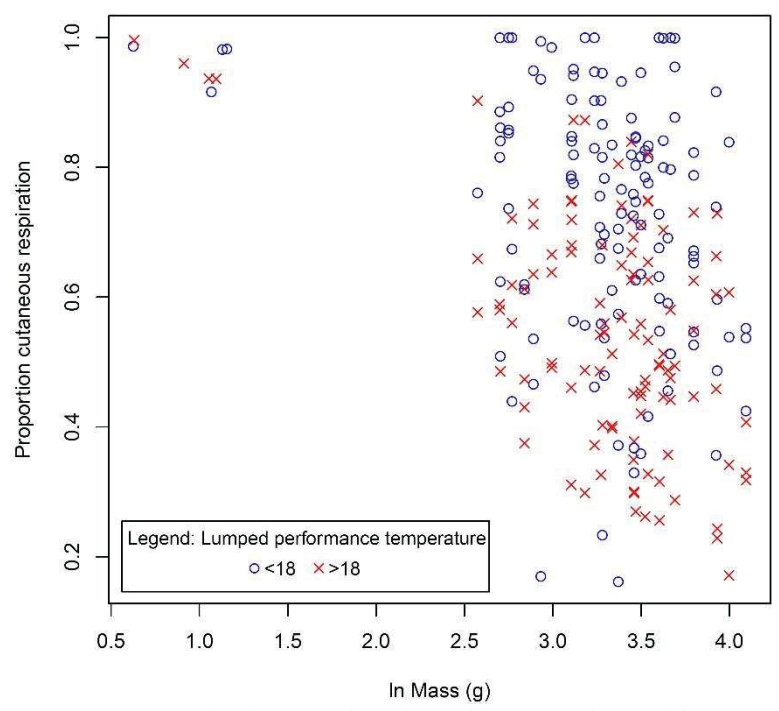


Figure S6 Proportion cutaneous respiration as a function of log-transformed frog mass, showing all measurements including the eight smaller frogs measured after the primary controlled-temperature experiment was completed. The eight smaller frogs exhibited an average of 96.2% cutaneous respiration, compared with an average of 63.7% cutaneous respiration for the larger frogs in the primary experiment. The color gradient shifts from coldest (8 °C; light blue) to warmest (29 °C; bright red) performance temperatures.

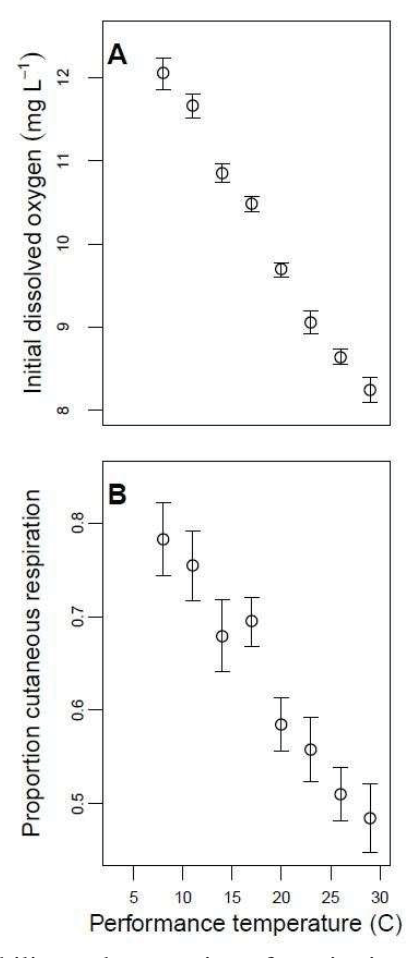


Figure S7 Dissolved oxygen availability and proportion of respiration performed cutaneously as functions of temperature in the primary controlled-temperature experiment. (A) Initial dissolved oxygen availability in water for each performance temperature across all time points. (B) Proportion of cutaneous respiration at each performance temperature across all data. Values are presented as mean \pm SE (N=228).